Supporting Information

New Genetically Engineered Derivatives of Antibacterial Darobactins Underpin their Potential for Antibiotic Development

Carsten E. Seyfert[a,b], Alison V. Müller[a,b], Danica J. Walsh[a,b], Joy Birkelbach[a,b], Andreas M. Kany[a,b], Christoph Porten[a,b], Biao Yuan[c,d,f], Daniel Krug[a,b], Jennifer Herrmann[a,b], Thomas C. Marlovits[c,d,f], Anna K. H. Hirsch[a,b,e] and Rolf Müller*[a,b,e]

[a]Helmholtz Institute for Pharmaceutical Research Saarland (HIPS), Helmholtz Centre for Infection Research (HZI) and Saarland University Department of Pharmacy, 66123 Saarbrücken, Germany

[b]German Centre for Infection Research (DZIF), partner site 38124 Hannover-Braunschweig, Germany

[c]University Medical Center Hamburg-Eppendorf (UKE), Institute of Structural and Systems Biology and Centre for Structural Systems Biology (CSSB), 22607 Hamburg, Germany

[d]Deutsches Elektronen-Synchrotron Zentrum (DESY), 22607 Hamburg, Germany

[e]Helmholtz International Lab for Anti-Infectives, 66123 Saarbrücken, Germany

[f]Centre for Structural Systems Biology (CSSB), 22607 Hamburg, Germany

Corresponding Author

*E.mail: rolf.mueller@helmholtz-hips.de. Phone: (+49)681 98806-3002

Table of Contents

Table of figures

List of tables

Structure-driven *in silico* design of new darobactin analogues

BamABCDE (BAM) – darobactin cryo-EM co-structures with the accession code 7NRI (**DA**), 8ADI (**D9**) and 8ADG (**D22**) were analyzed on their appropriate interaction site using Pymol 2.5.2 and ChimeraX1.3 software 1; 2. The Pymol "Mutagenesis" and the Chimera "rotamers" tool were used to exchange the asparagine on position 2 of the darobactin heptapeptide with proteinogenic amino acids of variable length and polarity.[1–3] The potential hydrogen bonding interactions were automatically computed in the respective structural analysis software.[2,4] The orientation of the changed amino acids was calculated by the automatic rotamer tool based on the probabilities of the rotamer library. Based on the findings, novel derivatives, potentially interacting with BamA, were designed and generated using the overlap-extension PCR method previously developed to generated darobactin **D22** to **D39**.[5] In brief, oligonucleotides harboring mismatches compared to the nucleotide core sequence of pNOSOdarABCDE-D22 were externally synthesized (Sigma-Aldrich) (Table S1). In two independent PCR reactions (PCR I, PCR II) fragments, harboring point mutations in the nucleotide core region, were amplified and used as templates for an overlapping PCR (PCR III) to combine the fragments of PCR I and PCR II. The combined fragments were separated via agarose gel electrophoresis, and purified using the NucleoSpin Gel and PCR Cleanup kit (Macherey-Nagel). The purified DNA fragments were digested using restriction-ligation based techniques to generate novel expression constructs summarized in Table S2.

Table S 1: Oligonucleotides used to mutate the *darA* core region for the generation of novel expression constructs with modified darobactin BGC.

Oligonucleotide name	Sequence (5'-3')	Function	Reference
pr1_dar9_fw	GGTGATGTCGGCGATATAGG	Primer for PCR I and III	Seyfert *et al.* 2022
pr1_dar9_v2_fw	GGTGATGTCGGCGATATAGGCG	Primer for PCR I and III	Seyfert *et al.* 2022
pr2_dar22_58b_rv	GCCACCGTTTAGTCCATTCCCAGGCCGT	Primer for PCR I to insert point mutation into *darA*	This study
pr2_dar22_59b_rv	GCCACCGTTTAGTCCATTTCCAGGCCGT	Primer for PCR I to insert point mutation into *darA*	This study
pr2_dar22_60_rv	GCCACCGTTTAGTCCAATCCCAGGCCGT	Primer for PCR I to insert point mutation into *darA*	This study
pr2_dar22_61_rv	GCCACCGTTTAGTCCATTGCCAGGCCGT	Primer for PCR I to insert point mutation into *darA*	This study
pr2_dar22_62_rv	GCCACCGTTTAGTCCATCTCCAGGCCGT	Primer for PCR I to insert point mutation into *darA*	This study
pr2_dar22_63_rv	GCCACCGTTTAGTCCAAACCCAGGCCGT	Primer for PCR I to insert point mutation into *darA*	This study
pr2_dar22_64_rv	GCCACCGTTTAGTCCATGACCAGGCCGT	Primer for PCR I to insert point mutation into *darA*	This study
pr2_dar22_65_rv	GCCATTTTTTAGTCCATGACCAGGCCGT	Primer for PCR I to insert point mutation into *darA*	This study
pr2_dar22_65_rv2	GCCATTTTTTAGTCCATGACCAGG	Primer for PCR I to insert point mutation into *darA*	This study
pr2_dar22_66_rv	AAATTTCCTGCCAACATTTAGTCCAGTTCCA	Primer for PCR I to insert point mutation into *darA*	This study
pr2_dar22_67_rv	GCCACCGTTTAGTCCAATACCAGGCCGT	Primer for PCR I to insert point mutation into *darA*	This study
pr2_dar22_68_rv	GCCACCGTTTAGTCCATAACCAGGCCGT	Primer for PCR I to insert point mutation into *darA*	This study
pr2_dar22_69_rv	GCCACCGTTTTGACCATTGCCAGGCCGT	Primer for PCR I to insert point mutation into *darA*	This study

pr2_dar22_70_rv	GCCACCGTTTTGACCA TGACCAGGCCGT	Primer for PCR I to insert point mutation into *darA*	This study
pr2_dar22_71_rv	GCCACCGTTTTGACCA TTCCCAGGCCGT	Primer for PCR I to insert point mutation into *darA*	This study
pr2_dar22_72_rv	GCCACCGTTTTGACCA TTTCCAGGCCGT	Primer for PCR I to insert point mutation into *darA*	This study
pr2_dar22_72_rv2	GCCACCGTTTTGACCA TTTCCAGGC	Primer for PCR I to insert point mutation into *darA*	This study
pr2_dar22_73_rv	GCCACCGTTTTGACCA ATCCCAGGCCGT	Primer for PCR I to insert point mutation into *darA*	This study
pr2_dar22_74_rv	AAATTTCCTGCCATTG TTTAGTCCAGTTCCA	Primer for PCR I to insert point mutation into *darA*	This study
pr3_dar9_Trp_fw	TGGCAGGAAATTTAAA GCTTATCCCAT	Primer for PCR II	Seyfert *et al.* 2022
pr3_dar22_v2_fw	CTAAACGGTGGCAGGA AATTTAAAGCTTATC	Primer for PCR II	Seyfert *et al.* 2022
pr3_dar65b_6K_fw	CTAAAAAATGGCAGGA AATTTAAAGCTTATCC CA	Primer for PCR II	This study
pr3_dar22_6C_fw	CTAAATGTTGGCAGGA AATTTAAAGCTTATC	Primer for PCR II	This study
pr3_dar22_4S_fw	CAAAACGGTGGCAGG AAATTTAAAGCTTATC	Primer for PCR II	This study
pr3_dar22_6Q_fw	CTAAACAATGGCAGGA AATTTAAAGCTTATC	Primer for PCR II	This study
pr4_dar9_rv	TGGGGATCCTCAGGAC TGCAG	Primer for PCR II and III	Seyfert *et al.* 2022

Table S 2: Expression plasmids generated to express and produce novel darobactins in *E. coli* BL21 (DE3).

Plasmid	**size [kb]**	**Relevant characteristics/ construction**	**Reference**
pNOSO-darABCDE-22	9.9	*E. coli* cloning and expression vector for production of **D22**	Seyfert *et al.*
pNOSO-darABCDE-58	9.9	*E. coli* cloning and expression vector for production of **D58**	This study
pNOSO-darABCDE-59	9.9	*E. coli* cloning and expression vector for production of **D59**	This study
pNOSO-darABCDE-60	9.9	*E. coli* cloning and expression vector for production of **D60**	This study
pNOSO-darABCDE-61	9.9	*E. coli* cloning and expression vector for production of **D61**	This study
pNOSO-darABCDE-62	9.9	*E. coli* cloning and expression vector for production of **D62**	This study
pNOSO-darABCDE-63	9.9	*E. coli* cloning and expression vector for production of **D63**	This study
pNOSO-darABCDE-64	9.9	*E. coli* cloning and expression vector for production of **D64**	This study
pNOSO-darABCDE-65	9.9	*E. coli* cloning and expression vector for production of **D65**	This study
pNOSO-darABCDE-66	9.9	*E. coli* cloning and expression vector for production of **D66**	This study
pNOSO-darABCDE-67	9.9	*E. coli* cloning and expression vector for production of **D67**	This study
pNOSO-darABCDE-68	9.9	*E. coli* cloning and expression vector for production of **D68**	This study

pNOSO-darABCDE-69	9.9	*E. coli* cloning and expression vector for production of **D69**	This study
pNOSO-darABCDE-70	9.9	*E. coli* cloning and expression vector for production of **D70**	This study
pNOSO-darABCDE-71	9.9	*E. coli* cloning and expression vector for production of **D71**	This study
pNOSO-darABCDE-72	9.9	*E. coli* cloning and expression vector for production of **D72**	This study
pNOSO-darABCDE-73	9.9	*E. coli* cloning and expression vector for production of **D73**	This study
pNOSO-darABCDE-74	9.9	*E. coli* cloning and expression vector for production of **D74**	This study

Table S 3: List of bacterial strains generated or used in this study.

Bacterial strain	Genotype	Reference
Cloning strains		
E. coli HS996	F^-, *mcr*A, Δ(*mrr-hsd*RMS-*mcr*BC), Φ80*lac*ZΔM15, Δ*lac*X74, *rec*A1, *ara*D139, Δ(*ara-leu*)7697, *gal*U, *gal*K, *rps*L (Str^R), *end*A1, *nup*G, *fhu*A::IS2	Invitrogen
E. coli NEB10β	*mcr*A, spoT1Δ(*mrr-hsd*RMS-*mcr*BC), Φ80d(*lac*ZΔM15)*rec*A1, *rel*A1, Δ*lac*X74, *rec*A1, *ara*D139, Δ(*ara-leu*)7697, *gal*K16, *gal*E15, *rps*L (Str^R), *end*A1, *nup*G, *fhu*A	New England Biolabs
E. coli BL21 (DE3)	$F^–$, *ompT, gal, dcm, lon,* Δ$hsdS_B(r_B^–m_B^–)$, λ(DE3 [*lacI lacUV5-T7p07 ind1 sam7 nin5*]), $[malB^+]_{K\text{-}12}(\lambda^S)$	Invitrogen
E. coli BL21-Gold (DE3)	*E. coli* B F– ompT hsdS(rB– mB–) dcm+ Tetr gal λ(DE3) endA	Agilent Technologies
E. coli NEB10β pNOSO-darABCDE-22	*E. coli* NEB10β with pNOSO-darABCDE-22, kan^R	Seyfert *et al.* 2022
E. coli HS996 pNOSO-darABCDE-58	*E. coli* HS996 with pNOSO-darABCDE-58, kan^R	This study
E. coli HS996 pNOSO-darABCDE-59	*E. coli* HS996 with pNOSO-darABCDE-59, kan^R	This study
E. coli HS996 pNOSO-darABCDE-60	*E. coli* HS996 with pNOSO-darABCDE-60, kan^R	This study
E. coli HS996 pNOSO-darABCDE-61	*E. coli* HS996 with pNOSO-darABCDE-61, kan^R	This study
E. coli HS996 pNOSO-darABCDE-62	*E. coli* HS996 with pNOSO-darABCDE-62, kan^R	This study
E. coli HS996 pNOSO-darABCDE-63	*E. coli* HS996 with pNOSO-darABCDE-63, kan^R	This study
E. coli HS996 pNOSO-darABCDE-64	*E. coli* HS996 with pNOSO-darABCDE-64, kan^R	This study
E. coli HS996 pNOSO-darABCDE-65	*E. coli* HS996 with pNOSO-darABCDE-65, kan^R	This study
E. coli HS996 pNOSO-darABCDE-66	*E. coli* HS996 with pNOSO-darABCDE-66, kan^R	This study
E. coli HS996 pNOSO-darABCDE-67	*E. coli* HS996 with pNOSO-darABCDE-67, kan^R	This study

E. coli HS996 pNOSO-darABCDE-68	*E. coli* HS996 with pNOSO-darABCDE-68, kan^R	This study
E. coli HS996 pNOSO-darABCDE-69	*E. coli* HS996 with pNOSO-darABCDE-69, kan^R	This study
E. coli HS996 pNOSO-darABCDE-70	*E. coli* HS996 with pNOSO-darABCDE-70, kan^R	This study
E. coli HS996 pNOSO-darABCDE-71	*E. coli* HS996 with pNOSO-darABCDE-71, kan^R	This study
E. coli HS996 pNOSO-darABCDE-72	*E. coli* HS996 with pNOSO-darABCDE-72, kan^R	This study
E. coli HS996 pNOSO-darABCDE-73	*E. coli* HS996 with pNOSO-darABCDE-73, kan^R	This study
E. coli HS996 pNOSO-darABCDE-74	*E. coli* HS996 with pNOSO-darABCDE-74, kan^R	This study
Heterologous producer strains		
E. coli BL21 (DE3) pNOSO-darABCDE-22	*E. coli* BL21 (DE3) with pNOSO-darABCDE-22, kan^R	This study
E. coli BL21-Gold (DE3) pNOSO-darABCDE-22	*E. coli* BL21-Gold (DE3) with pNOSO-darABCDE-22, kan^R	This study
E. coli BL21 (DE3) pNOSO-darABCDE-58	*E. coli* BL21 (DE3) with pNOSO-darABCDE-58, kan^R	This study
E. coli BL21 (DE3) pNOSO-darABCDE-59	*E. coli* BL21 (DE3) with pNOSO-darABCDE-59, kan^R	This study
E. coli BL21 (DE3) pNOSO-darABCDE-60	*E. coli* BL21 (DE3) with pNOSO-darABCDE-60, kan^R	This study
E. coli BL21 (DE3) pNOSO-darABCDE-61	*E. coli* BL21 (DE3) with pNOSO-darABCDE-61, kan^R	This study
E. coli BL21 (DE3) pNOSO-darABCDE-62	*E. coli* BL21 (DE3) with pNOSO-darABCDE-62, kan^R	This study
E. coli BL21 (DE3) pNOSO-darABCDE-63	*E. coli* BL21 (DE3) with pNOSO-darABCDE-63, kan^R	This study
E. coli BL21 (DE3) pNOSO-darABCDE-64	*E. coli* BL21 (DE3) with pNOSO-darABCDE-64, kan^R	This study
E. coli BL21 (DE3) pNOSO-darABCDE-65	*E. coli* BL21 (DE3) with pNOSO-darABCDE-65, kan^R	This study
E. coli BL21 (DE3) pNOSO-darABCDE-66	*E. coli* BL21 (DE3) with pNOSO-darABCDE-66, kan^R	This study
E. coli BL21 (DE3) pNOSO-darABCDE-67	*E. coli* BL21 (DE3) with pNOSO-darABCDE-67, kan^R	This study
E. coli BL21 (DE3) pNOSO-darABCDE-68	*E. coli* BL21 (DE3) with pNOSO-darABCDE-68, kan^R	This study
E. coli BL21 (DE3) pNOSO-darABCDE-69	*E. coli* BL21 (DE3) with pNOSO-darABCDE-69, kan^R	This study
E. coli BL21 (DE3) pNOSO-darABCDE-70	*E. coli* BL21 (DE3) with pNOSO-darABCDE-70, kan^R	This study
E. coli BL21 (DE3) pNOSO-darABCDE-71	*E. coli* BL21 (DE3) with pNOSO-darABCDE-71, kan^R	This study
E. coli BL21 (DE3) pNOSO-darABCDE-72	*E. coli* BL21 (DE3) with pNOSO-darABCDE-72, kan^R	This study
E. coli BL21 (DE3) pNOSO-darABCDE-73	*E. coli* BL21 (DE3) with pNOSO-darABCDE-73, kan^R	This study
E. coli BL21 (DE3) pNOSO-darABCDE-74	*E. coli* BL21 (DE3) with pNOSO-darABCDE-74, kan^R	This study

E. coli BL21 (λ DE3) Lemo cells pET15b-BamAβ421-810	*E. coli* BL21 (λ DE3) Lemo cells with pET15b-BamAβ421-810, amp^R	Seyfert *et al.* 2022

Supplementation figures and tables

1. Mutagenesis of the darobactin heptapeptide

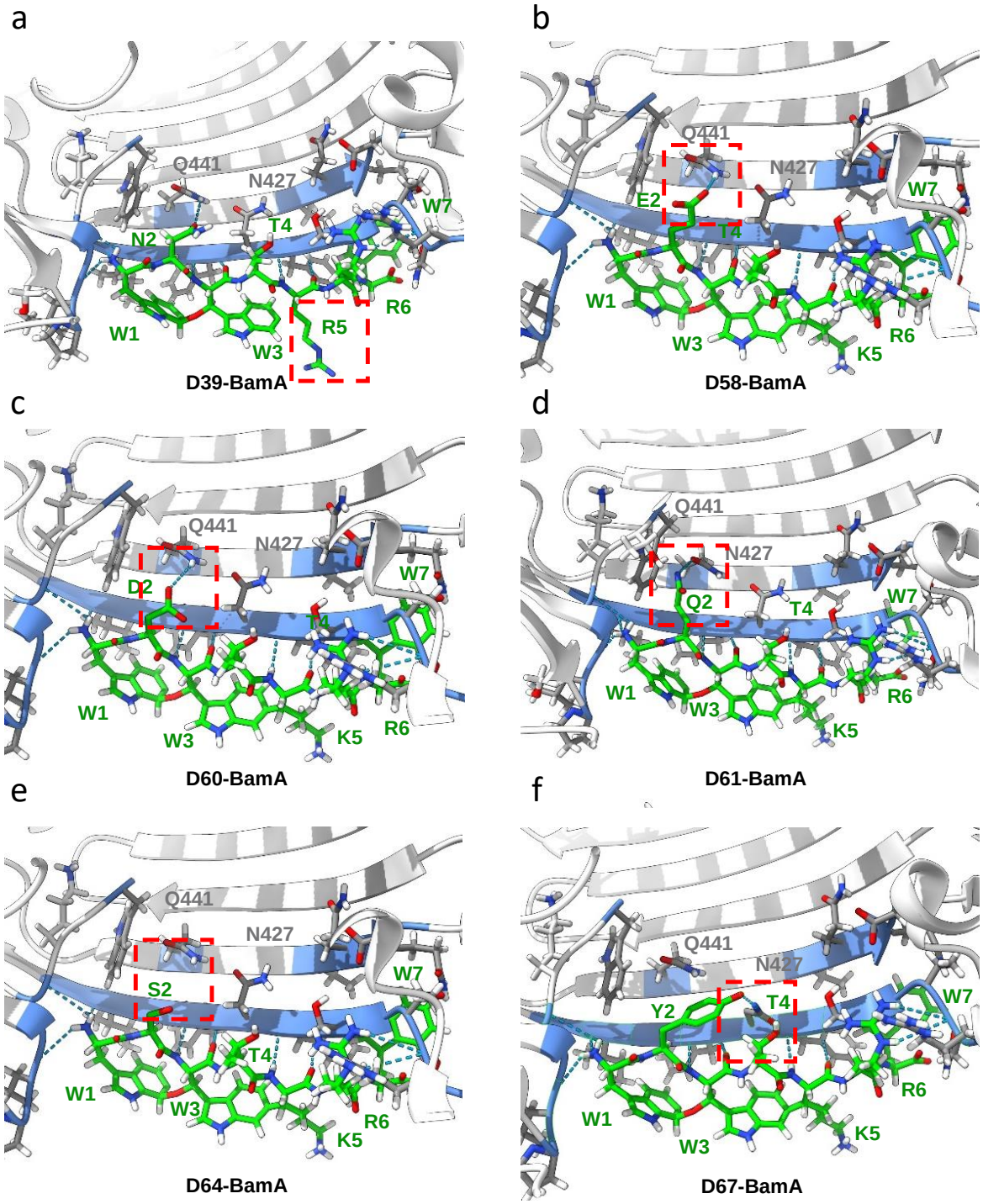

Figure S 1: Mutagenesis of D22 bound to BamABCDE to predict the possible interaction of D39, D58, D60, D61, D64 and D67 with BamA. Chimera rotamer tool was used to model potential hydrogen bonding interactions by changing a) L-arginine to L- lysine to project **D38**-BamA interaction b) L-asparagine to L-glutamic acid to project **D58**-BamA interaction c) L- asparagine to L-aspartic acid to project **D60**-BamA interaction d) L-asparagine to L-glutamine to project **D61**-BamA interaction e) L-asparagine to L-serine to project **D64**-BamA interaction f) L-asparagine to L-tyrosine to project **D67**-BamA interaction. Changes and modeled interactions were highlighted in red. The raw data of **D22** were taken from protein data bank (PDB) for the mutagenesis and were originally published in Seyfert *et al*.[5] with the PDB accession code: 8ADG (D22).

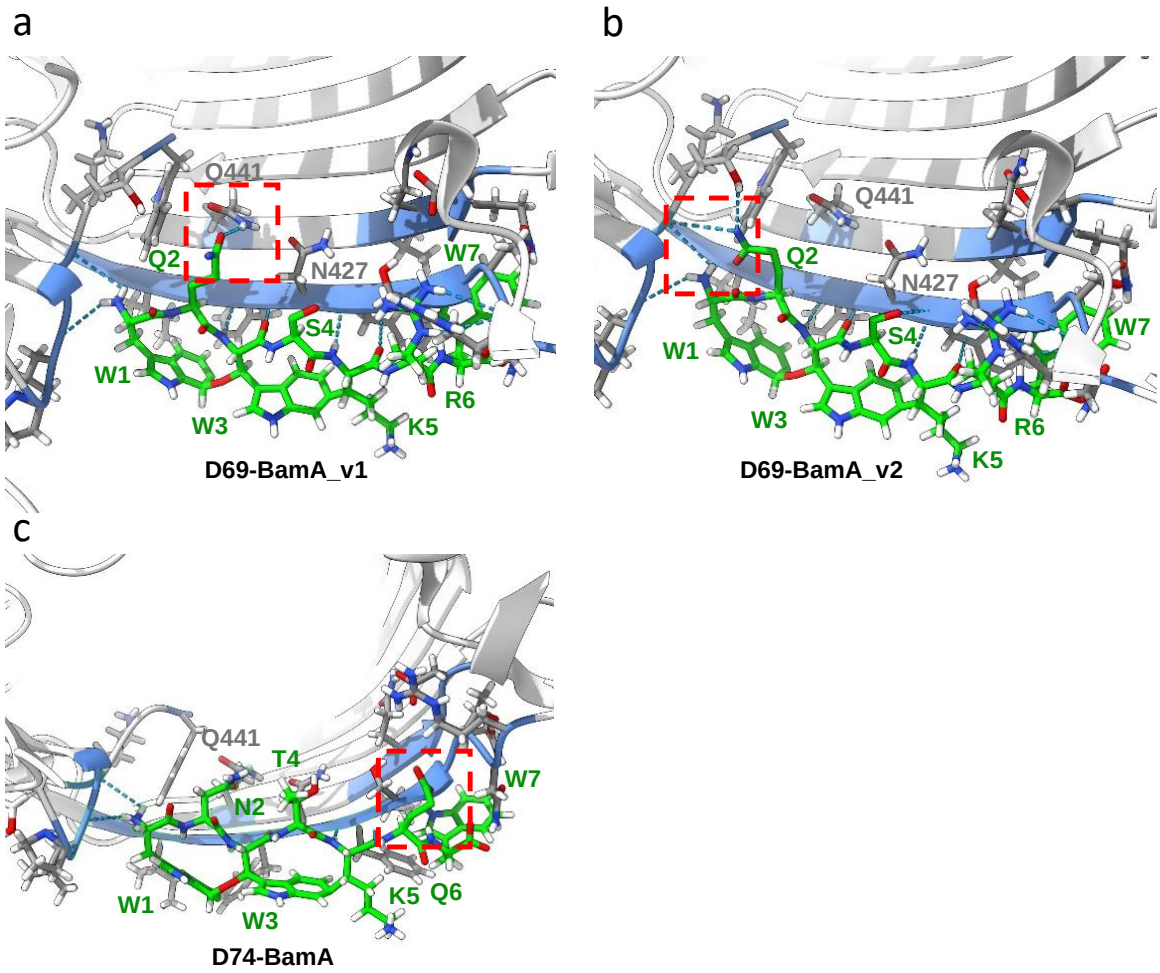

Figure S 2: Mutagenesis of D22 bound to BamABCDE to predict the possible interaction of D69 and D74 with BamA. Chimera rotamer tool was used to model the interactions by changing of a) and b) L-asparagine to L-glutamine to project **D69**-BamA interaction c) L-arginine to L-glutamine to project **D74**-BamA interaction. Changes and modeled interactions were highlighted in red. The raw data of **D22** were taken from protein data bank (PDB) as starting point for molecular modeling. The accession code is 8ADG (**D22**).

2. Chromatograms of darobactin extracts

Table S 4: The calculated (calc.) and observed (obs.) masses of the darobactin analogues. The core peptide sequence of each new derivative with highlighted (red) differences in the core peptide compared to **D22** is indicated. The calc. and obs. masses in the extracts of the different charge states ($[M+H]^{1+}$, $[M+2H]^{2+}$ and $[M+3H]^{3+}$) for each derivative are listed.

Darobactin analogue	Core peptide	Calc. mass $[M+H]^{1+}$	Obs. mass $[M+H]^{1+}$	Calc. mass $[M+2H]^{2+}$	Obs. mass $[M+2H]^{2+}$	Calc. mass $[M+3H]^{3+}$	Obs. mass $[M+3H]^{3+}$	Calc. mass $[M+3H-NH_3]^{3+}$	Obs. mass $[M+3H-NH_3]^{3+}$
D58	W E W T K R W	1103.5058	1103.5171	552.2565	552.2632	368.5068	368.5109	362.8318	362.8351
D59	W K W T K R W	1102.5582	1102.4853	551.7827	551.7889	368.1909	368.1951	362.5159	362.5204
D60	W D W T K R W	1089.4901	1089.5022	545.2487	545.2555	363.8349	363.8392	358.1599	358.1636
D61	W Q W T K R W	1102.5218	1102.5318	551.7645	551.7711	368.1788	368.1831	362.5038	362.5073
D62	W R W T K R W	1130.5643	1130.5152	565.7858	565.7906	377.5263	377.5306	371.8513	371.8691
D63	W V W T K R W	1073.5316	1073.5133	537.2694	537.2752	358.5154	358.1436	352.8404	352.8433
D64	W S W T K R W	1061.4952	1061.5028	531.2512	531.2575	354.5033	354.5071	348.8283	348.8315
D65	W S W T K K W	1033.4891	1033.4981	517.2482	517.2535	345.1679	345.1713	339.4929	339.4956
D66	W N W T K C W	1226.4394	1226.4533	613.7207	613.7307	409.4896	409.4887	403.8146	403.8122
D67	W Y W T K R W	1137.5265	1137.5359	569.2669	569.2734	379.8470	379.8510	374.1720	374.1754
D68	W L W T K R W	1087.5473	1087.5103	544.2773	544.2830	363.1873	363.1909	357.5123	357.5151
D69	W Q W S K R W	1088.5061	1088.5114	544.7567	544.7603	363.5069	363.5092	357.8319	357.8334
D70	W S W S K R W	1047.4796	1047.4822	524.2434	524.2461	349.8314	349.8328	344.1564	344.1574
D71	W E W S K R W	1089.4901	1089.4893	545.2487	545.2491	363.8349	363.8350	358.1599	358.1593
D72	W K W S K R W	1088.5425	1088.4476	544.7749	544.7741	363.5190	363.5184	357.8440	357.8430
D73	W D W S K R W	1075.4745	1075.4735	538.2409	538.2413	359.1630	359.1631	353.4880	353.4876
D74	W N W T K Q W	1060.4636	1060.4622	530.7354	530.7372	354.1594	354.1588	348.4844	348.4836

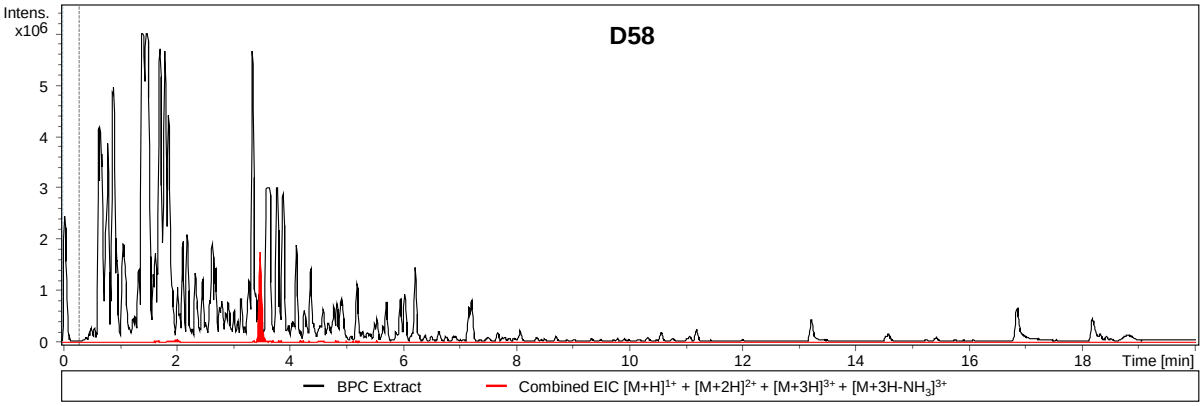

Figure S 3: Chromatogram of the *E. coli* BL21 (DE3) pNOSO-darABCDE-58 extract. The red trace shows the combined EIC for the $[M+H]^{1+}$, $[M+2H]^{2+}$, $[M+3H]^{3+}$ and $[M+3H\text{-}NH_3]^{3+}$ species of **D58** at their calculated masses, respectively (**Table S 4**) ±0.02 Da. The BPC of the whole extract from fermentation broth supernatant is presented in black.

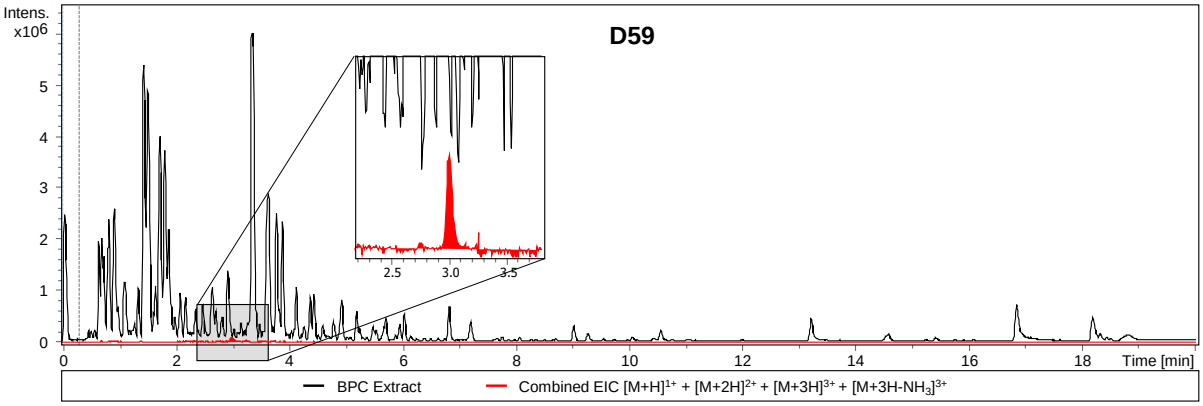

Figure S 4: Chromatogram of the *E. coli* BL21 (DE3) pNOSO-darABCDE-59 extract. The red trace shows the combined EIC for the $[M+H]^{1+}$, $[M+2H]^{2+}$, $[M+3H]^{3+}$ and $[M+3H\text{-}NH_3]^{3+}$ species of **D59** at their calculated masses, respectively (**Table S 4**) ±0.02 Da. The BPC of the whole extract from fermentation broth supernatant is presented in black.

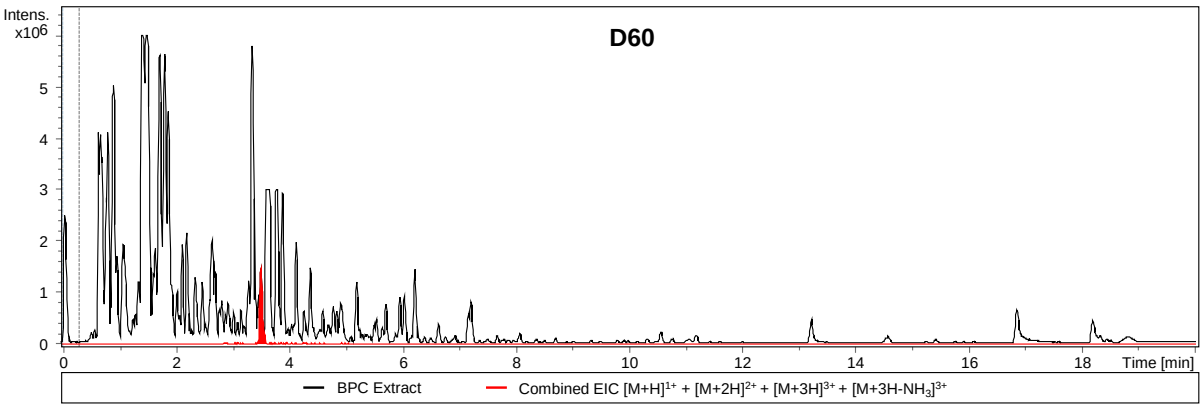

Figure S 5: Chromatogram of the *E. coli* BL21 (DE3) pNOSO-darABCDE-60 extract. The red trace shows the combined EIC for the $[M+H]^{1+}$, $[M+2H]^{2+}$, $[M+3H]^{3+}$ and $[M+3H\text{-}NH_3]^{3+}$ species of **D60** at their calculated masses, respectively (**Table S 4**) ±0.02 Da. The BPC of the whole extract from fermentation broth supernatant is presented in black.

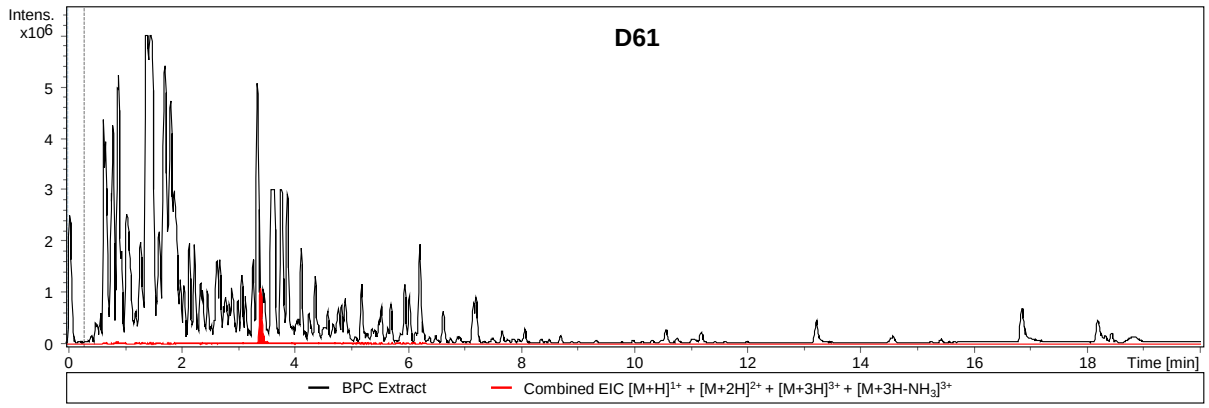

Figure S 6: Chromatogram of the *E. coli* BL21 (DE3) pNOSO-darABCDE-61 extract. The red trace shows the combined EIC for the $[M+H]^{1+}$, $[M+2H]^{2+}$, $[M+3H]^{3+}$ and $[M+3H\text{-}NH_3]^{3+}$ species of **D61** at their calculated masses, respectively (**Table S 4**) ±0.02 Da. The BPC of the whole extract from fermentation broth supernatant is presented in black.

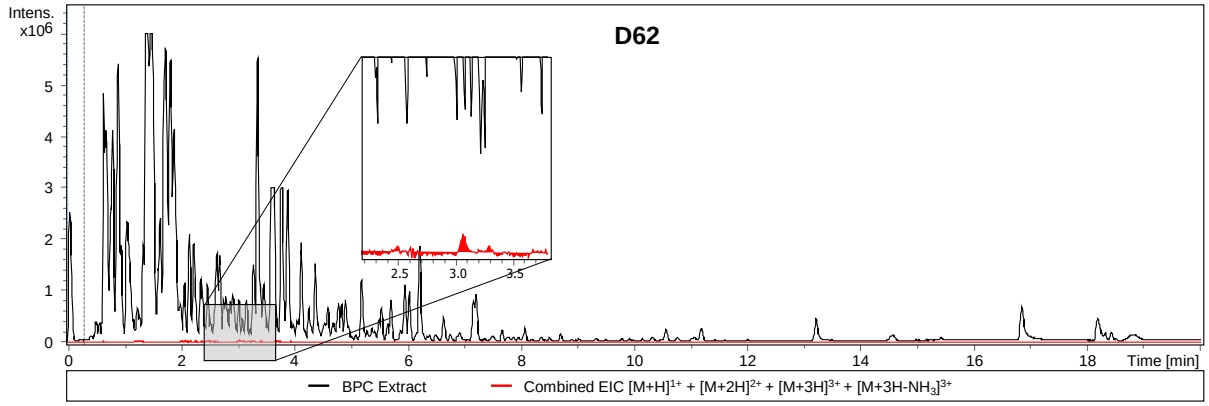

Figure S 7: Chromatogram of the *E. coli* BL21 (DE3) pNOSO-darABCDE-62 extract. The red trace shows the combined EIC for the $[M+H]^{1+}$, $[M+2H]^{2+}$, $[M+3H]^{3+}$ and $[M+3H\text{-}NH_3]^{3+}$ species of **D62** at their calculated masses, respectively (**Table S 4**) ±0.02 Da. The BPC of the whole extract from fermentation broth supernatant is presented in black.

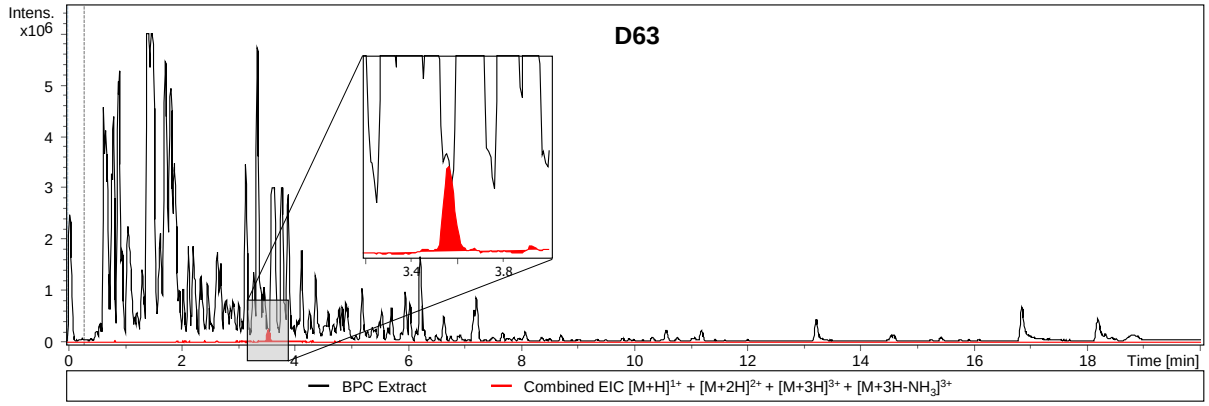

Figure S 8: Chromatogram of the *E. coli* BL21 (DE3) pNOSO-darABCDE-63 extract. The red trace shows the combined EIC for the $[M+H]^{1+}$, $[M+2H]^{2+}$, $[M+3H]^{3+}$ and $[M+3H\text{-}NH_3]^{3+}$ species of **D63** at their calculated masses, respectively (**Table S 4**) ±0.02 Da. The BPC of the whole extract from fermentation broth supernatant is presented in black.

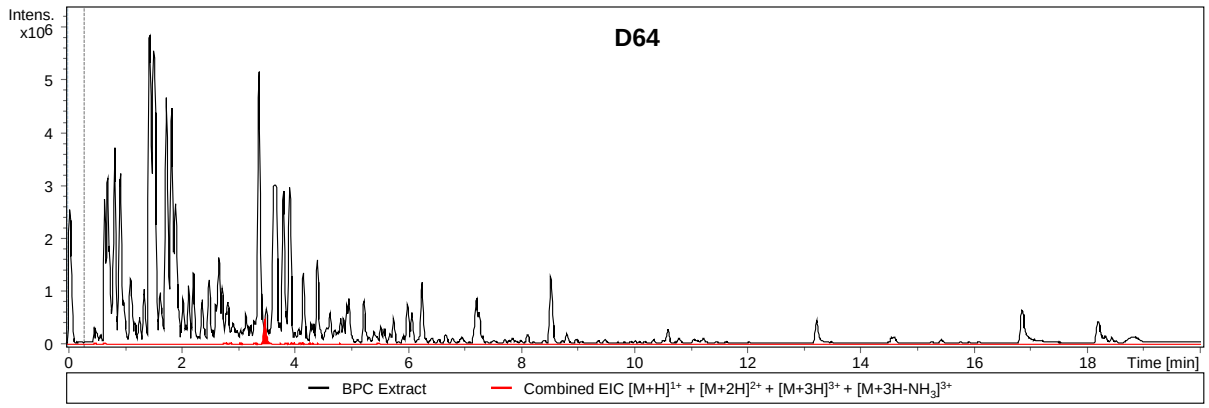

Figure S 9: Chromatogram of the *E. coli* BL21 (DE3) pNOSO-darABCDE-64 extract. The red trace shows the combined EIC for the $[M+H]^{1+}$, $[M+2H]^{2+}$, $[M+3H]^{3+}$ and $[M+3H\text{-}NH_3]^{3+}$ species of **D64** at their calculated masses, respectively (**Table S 4**) ±0.02 Da. The BPC of the whole extract from fermentation broth supernatant is presented in black.

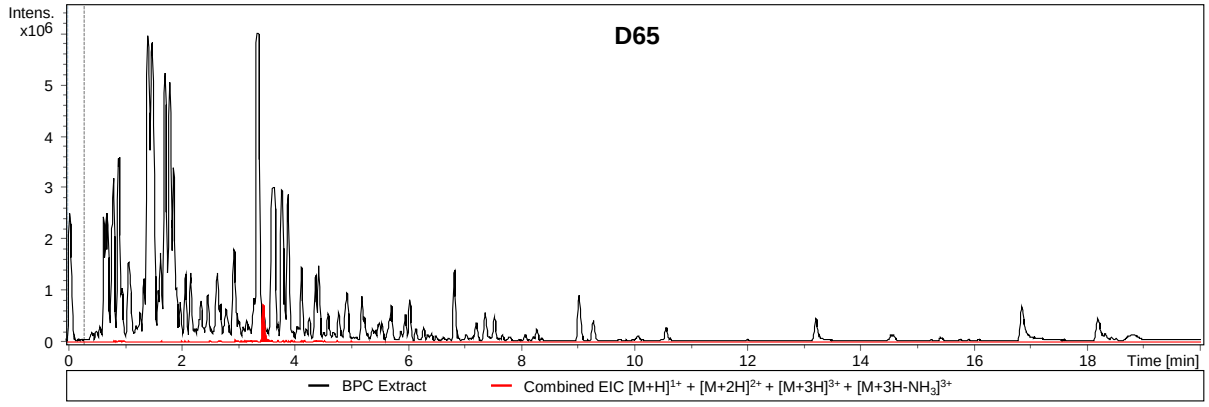

Figure S 10: Chromatogram of the *E. coli* BL21 (DE3) pNOSO-darABCDE-65 extract. The red trace shows the combined EIC for the $[M+H]^{1+}$, $[M+2H]^{2+}$, $[M+3H]^{3+}$ and $[M+3H\text{-}NH_3]^{3+}$ species of **D65** at their calculated masses, respectively (**Table S 4**) ±0.02 Da. The BPC of the whole extract from fermentation broth supernatant is presented in black.

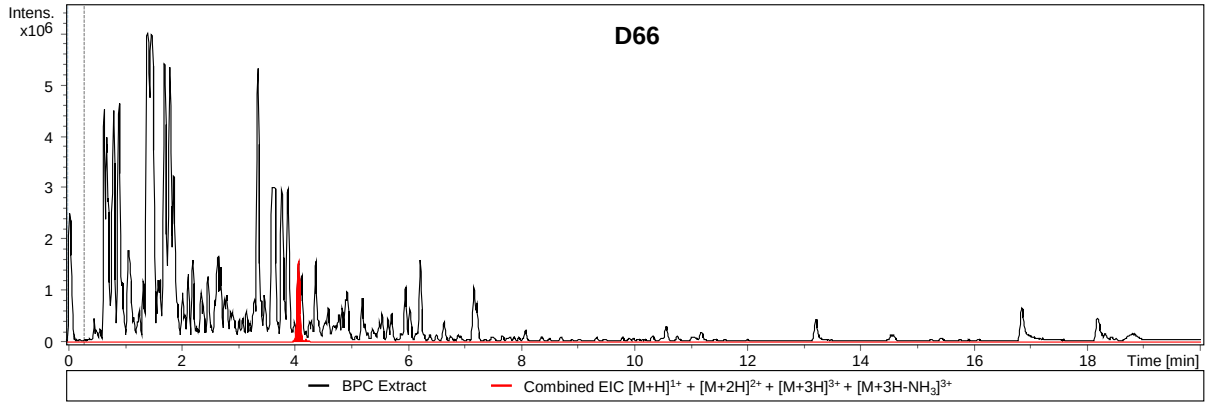

Figure S 11: Chromatogram of the *E. coli* BL21 (DE3) pNOSO-darABCDE-66 extract. The red trace shows the combined EIC for the $[M+H]^{1+}$, $[M+2H]^{2+}$, $[M+3H]^{3+}$ and $[M+3H\text{-}NH_3]^{3+}$ species of **D66** at their calculated masses, respectively (Table S 4) ±0.02 Da. The BPC of the whole extract from fermentation broth supernatant is presented in

black. , The L-cysteine of **D66** is linked to another L-cysteine and lactic acid via a disulfide bond (Table S 5, Figure S 11 and S 29), as was shown for **D6** and **D32** in previous studies.[5,6]

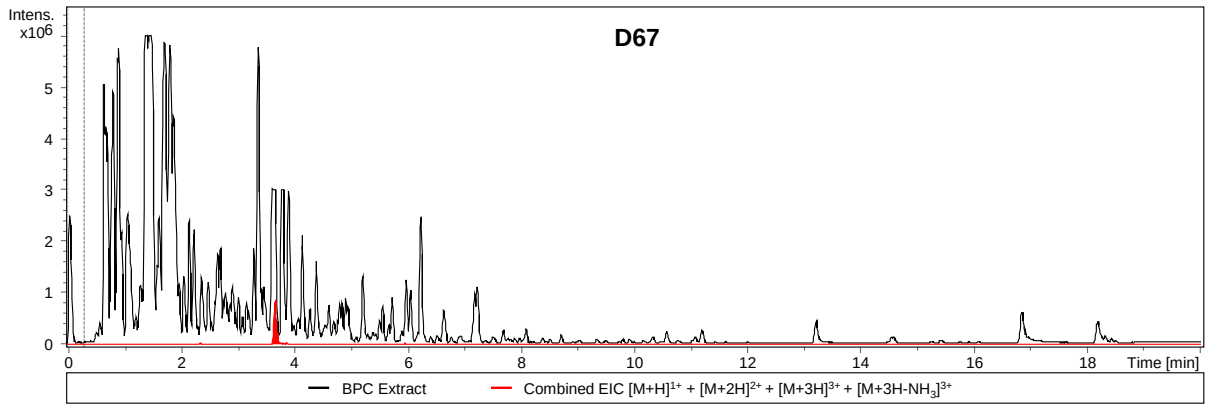

Figure S 12: Chromatogram of the *E. coli* BL21 (DE3) pNOSO-darABCDE-67 extract. The red trace shows the combined EIC for the $[M+H]^{1+}$, $[M+2H]^{2+}$, $[M+3H]^{3+}$ and $[M+3H\text{-}NH_3]^{3+}$ species of **D67** at their calculated masses, respectively (**Table S 4**) ±0.02 Da. The BPC of the whole extract from fermentation broth supernatant is presented in black.

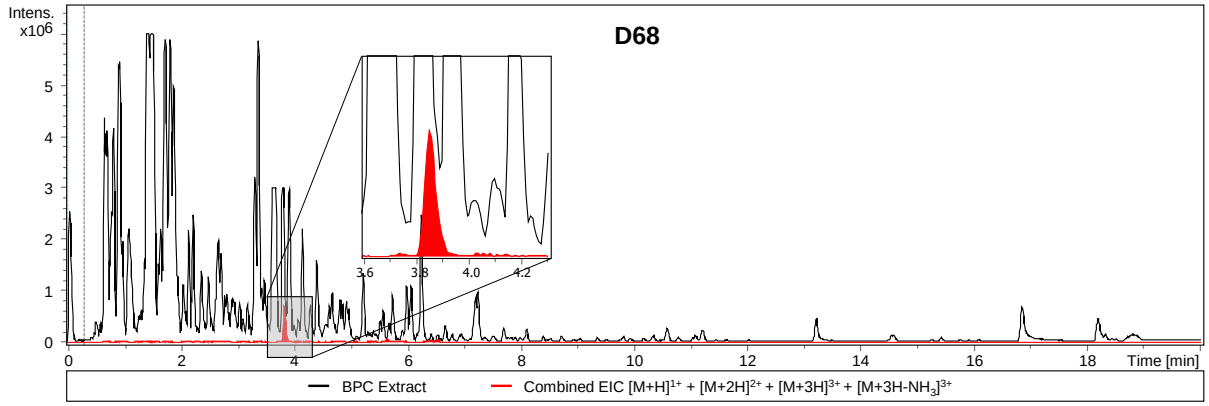

Figure S 13: Chromatogram of the *E. coli* BL21 (DE3) pNOSO-darABCDE-68 extract. The red trace shows the combined EIC for the $[M+H]^{1+}$, $[M+2H]^{2+}$, $[M+3H]^{3+}$ and $[M+3H\text{-}NH_3]^{3+}$ species of **D68** at their calculated masses, respectively (**Table S 4**) ±0.02 Da. The BPC of the whole extract from fermentation broth supernatant is presented in black.

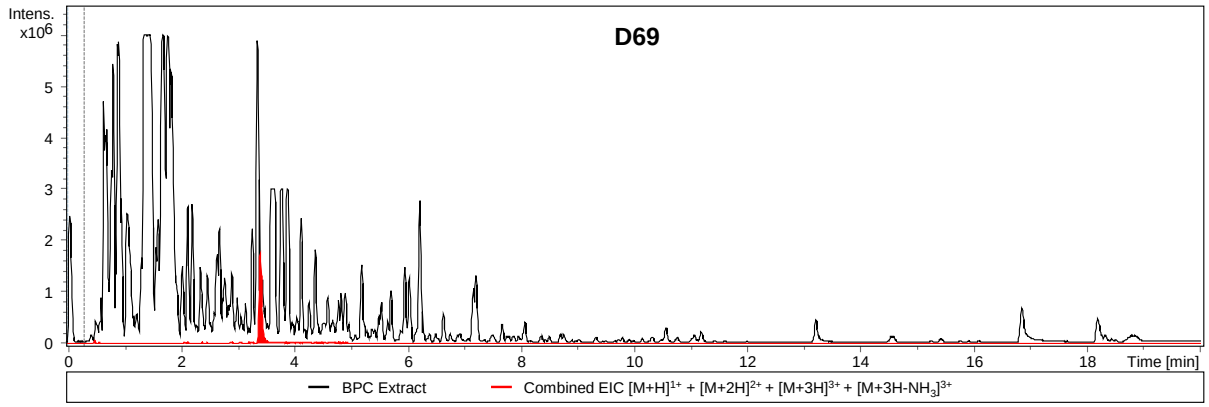

Figure S 14: Chromatogram of the *E. coli* BL21 (DE3) pNOSO-darABCDE-69 extract. The red trace shows the combined EIC for the $[M+H]^{1+}$, $[M+2H]^{2+}$, $[M+3H]^{3+}$ and $[M+3H\text{-}NH_3]^{3+}$ species of **D69** at their calculated masses, respectively (**Table S 4**) ±0.02 Da. The BPC of the whole extract from fermentation broth supernatant is presented in black.

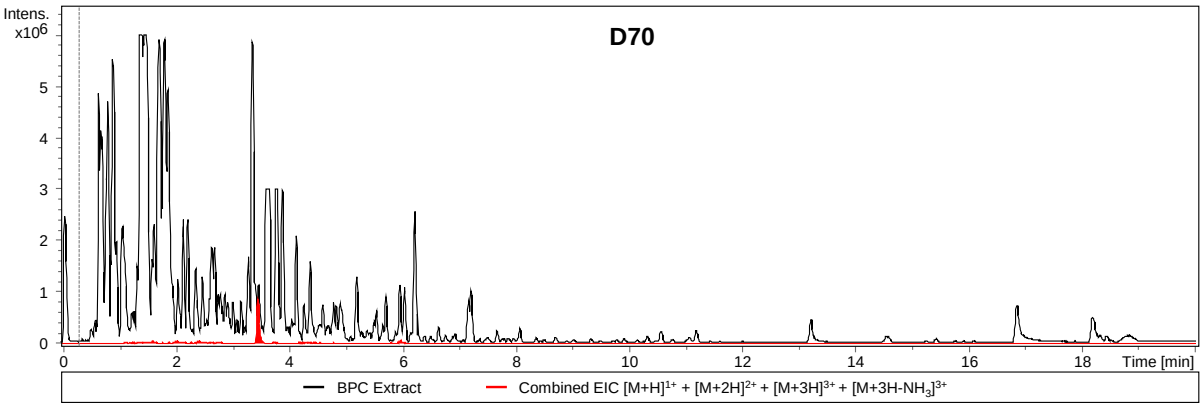

Figure S 15: Chromatogram of the *E. coli* BL21 (DE3) pNOSO-darABCDE-70 extract. The red trace shows the combined EIC for the $[M+H]^{1+}$, $[M+2H]^{2+}$, $[M+3H]^{3+}$ and $[M+3H\text{-}NH_3]^{3+}$ species of **D70** at their calculated masses, respectively (**Table S 4**) ±0.02 Da. The BPC of the whole extract from fermentation broth supernatant is presented in black.

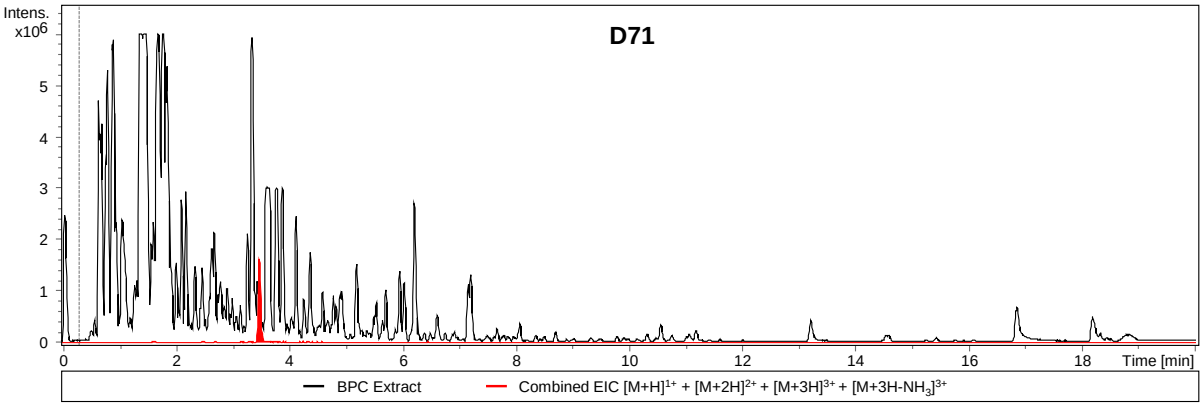

Figure S 16: Chromatogram of the *E. coli* BL21 (DE3) pNOSO-darABCDE-71 extract. The red trace shows the combined EIC for the $[M+H]^{1+}$, $[M+2H]^{2+}$, $[M+3H]^{3+}$ and $[M+3H\text{-}NH_3]^{3+}$ species of **D71** at their calculated masses, respectively (**Table S 4**) ±0.02 Da. The BPC of the whole extract from fermentation broth supernatant is presented in black.

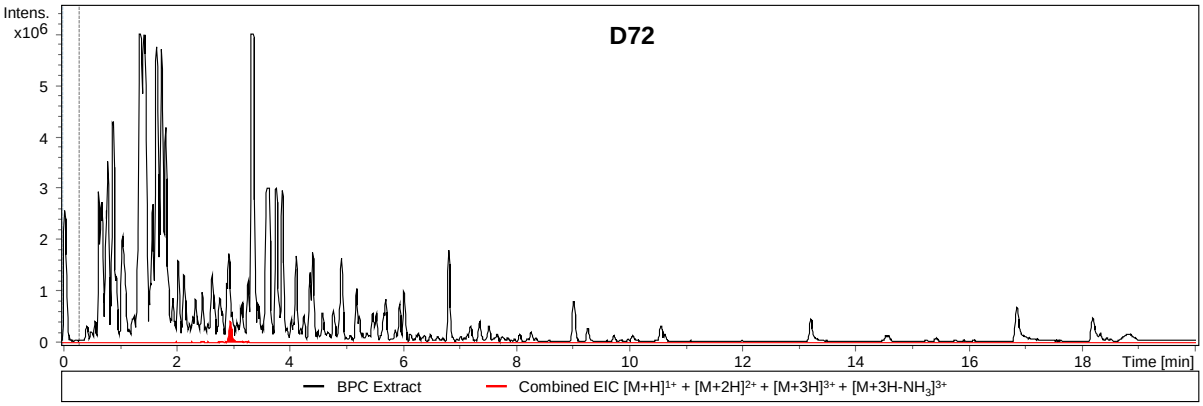

Figure S 17: Chromatogram of the *E. coli* BL21 (DE3) pNOSO-darABCDE-72 extract. The red trace shows the combined EIC for the $[M+H]^{1+}$, $[M+2H]^{2+}$, $[M+3H]^{3+}$ and $[M+3H\text{-}NH_3]^{3+}$ species of **D72** at their calculated masses, respectively (**Table S 4**) ±0.02 Da. The BPC of the whole extract from fermentation broth supernatant is presented in black.

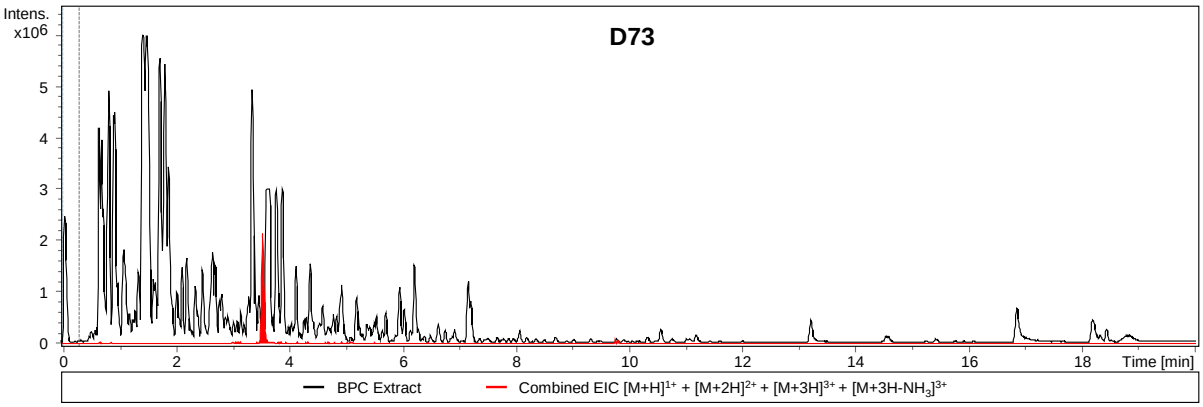

Figure S 18: Chromatogram of the *E. coli* BL21 (DE3) pNOSO-darABCDE-73 extract. The red trace shows the combined EIC for the $[M+H]^{1+}$, $[M+2H]^{2+}$, $[M+3H]^{3+}$ and $[M+3H\text{-}NH_3]^{3+}$ species of **D73** at their calculated masses, respectively (**Table S 4**) ±0.02 Da. The BPC of the whole extract from fermentation broth supernatant is presented in black.

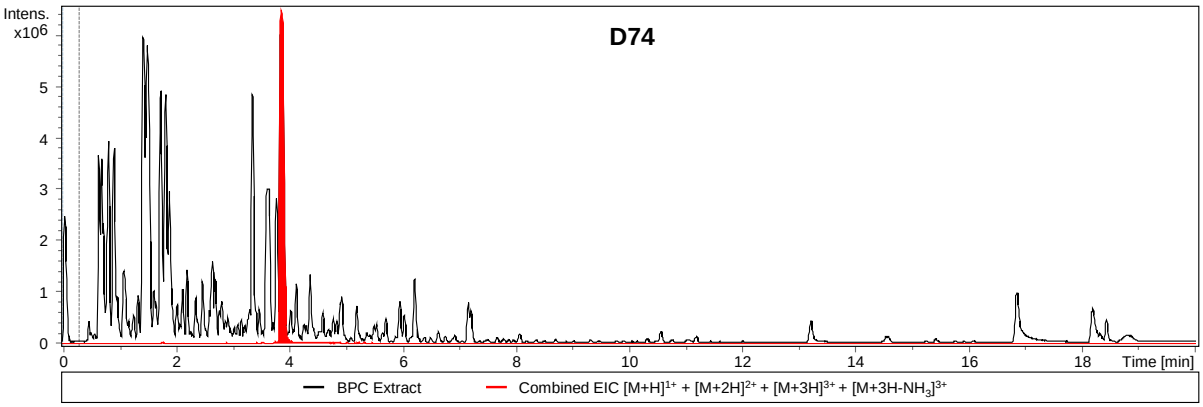

Figure S 19: Chromatogram of the *E. coli* BL21 (DE3) pNOSO-darABCDE-74 extract. The red trace shows the combined EIC for the $[M+H]^{1+}$, $[M+2H]^{2+}$, $[M+3H]^{3+}$ and $[M+3H\text{-}NH_3]^{3+}$ species of **D74** at their calculated masses, respectively (**Table S 4**) ±0.02 Da. The BPC of the whole extract from fermentation broth supernatant is presented in black.

3. MS^2 spectra analysis of darobactin analogues

The MS^2 spectra of all novel darobactin analogues are shown in Figure S 21-37. The blue quadratic symbols display the precursor ion, which was picked for fragmentation. The $[M\text{-}NH_3+2H]^{2+}$ fragment and the derivative related typical b2-ion with ammonia loss can be observed and allow the further verification of modifications (Figure S 20). The theoretical mass of all derivatives and the ions for the most characteristic fragmentation pattern are displayed in table S 5.

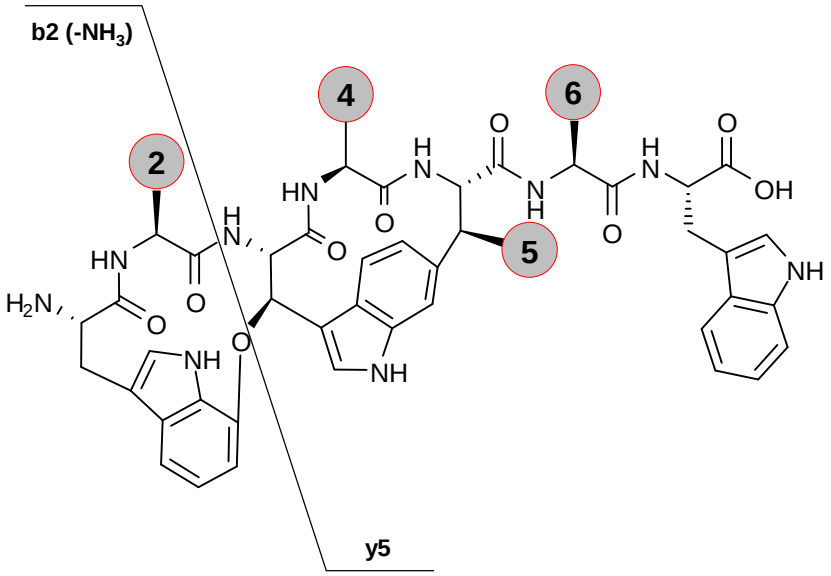

Figure S 20: MS^2 fragmentation pattern of darobactin analogues. The most characteristic ions in the MS^2 fragmentation pattern (b2 with or without ammonia loss and y5) are calculated and observed as described in the methods and displayed in Table S 5.

Table S 5: Calculated (calc.) and observed (obs.) masses of the typical b2 and y5 fragment ions. The novel darobactins with highlighted modifications in the core peptide in comparison to **D22** are summarized (differences in red). The calc. and obs. masses in the extracts of the $[M\text{-}NH_3+2H]^{2+}$ and the calc. and obs. typical b2 and y5 ion masses with ammonia loss are displayed.

Darobactin	Core peptide	calc. $[M\text{-}NH_3+2H]^{2+}$	obs. $[M\text{-}NH_3+2H]^{2+}$	calc. b2 – NH_3	obs. b2 – NH_3	calc. y5	obs. y5
58	W E W T K R W	543.7432	543.7384	315.0975	315.0959	772.3889	772.3822
59	W K W T K R W	543.2694	543.2674	314.1499	314.1434	772.3889	772.3831
60	W D W T K R W	536.7354	536.7287	301.0819	301.0796	772.3889	772.3799
61	W Q W T K R W	543.2512	543.2455	314.1135	314.1119	772.3889	772.3828
62	W R W T K R W	557.2673	557.2682	342.1561	342.1489	772.3889	772.3765
63	W V W T K R W	528.7561	528.7522	285.1234	285.1204	772.3889	772.3851
64	W S W T K R W	522.7380	522.7348	273.0870	273.0871	772.3889	772.3789
65	W S W T K K W	508.7349	508.7324	273.0870	273.1228	744.3828	744.3780
66	W N W T K C W	605.2012	605.2035	300.0979	300.0957	910.3222	910.3113
67	W Y W T K R W	560.7536	560.7478	349.1183	349.1139	772.3889	772.3809
68	W L W T K R W	535.7640	535.7581	299.1390	299.1383	772.3889	772.3808
69	W Q W S K R W	536.2434	536.2369	314.1135	314.1114	758.3733	758.3649
70	W S W S K R W	515.7301	515.7247	273.0870	273.0859	758.3733	758.3635
71	W E W S K R W	536.7354	536.7316	315.0975	315.0965	758.3733	758.3684
72	W K W S K R W	536.2616	536.2589	314.1499	314.1817	758.3733	758.3697
73	W D W S K R W	529.7276	529.7237	301.0819	301.0807	758.3733	758.3672
74	W N W T K Q W	522.2221	522.2198	300.0979	300.0967	744.3464	744.3422

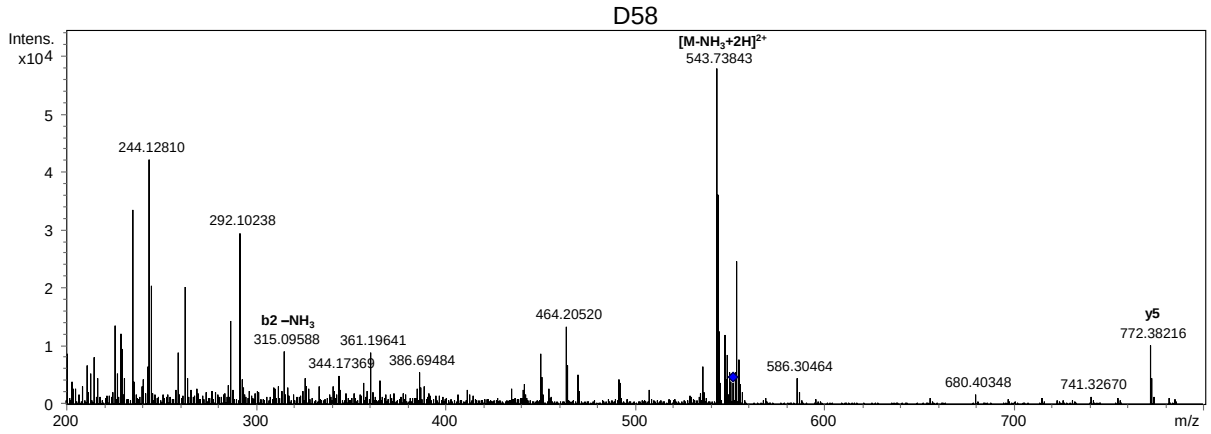

Figure S 21: MS^2 spectrum for D58.

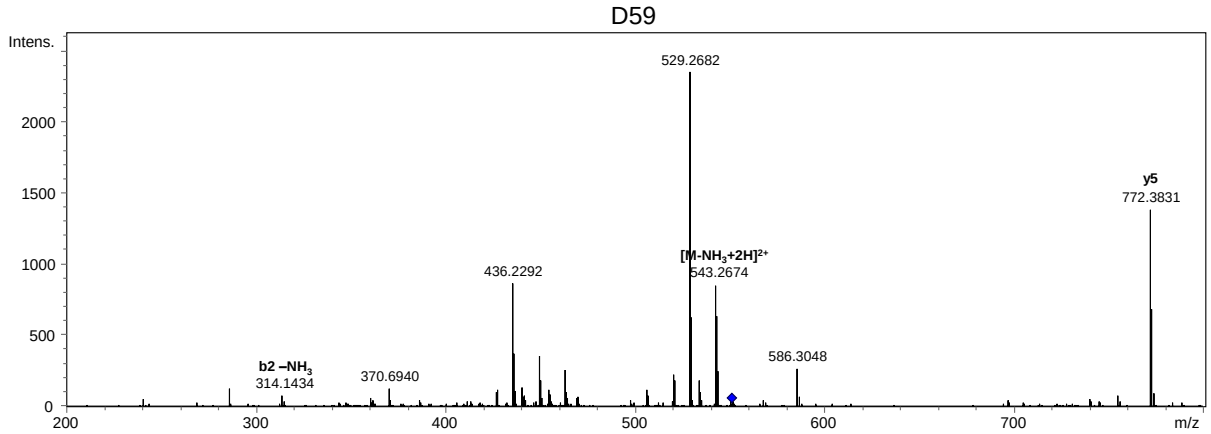

Figure S 22: MS^2 spectrum for D59.

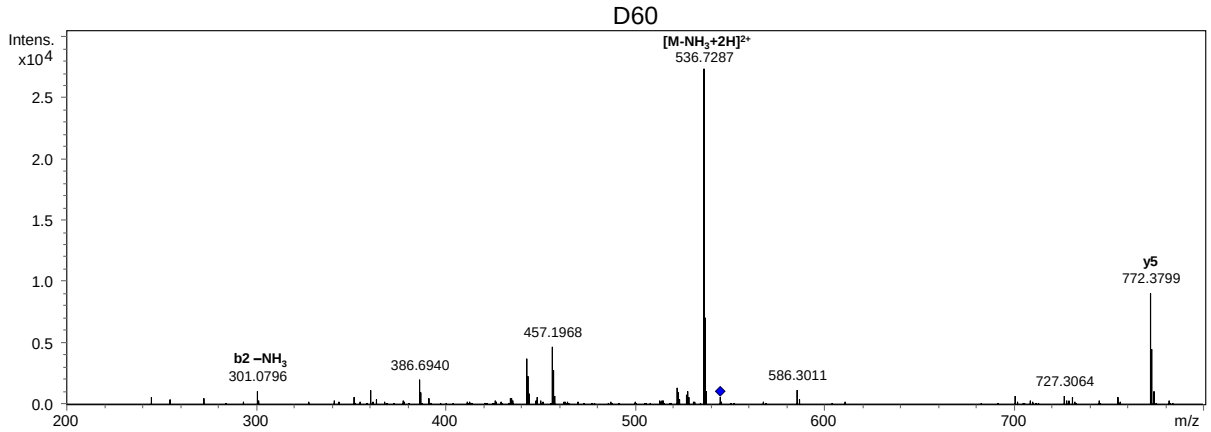

Figure S 23: MS^2 spectrum for D60.

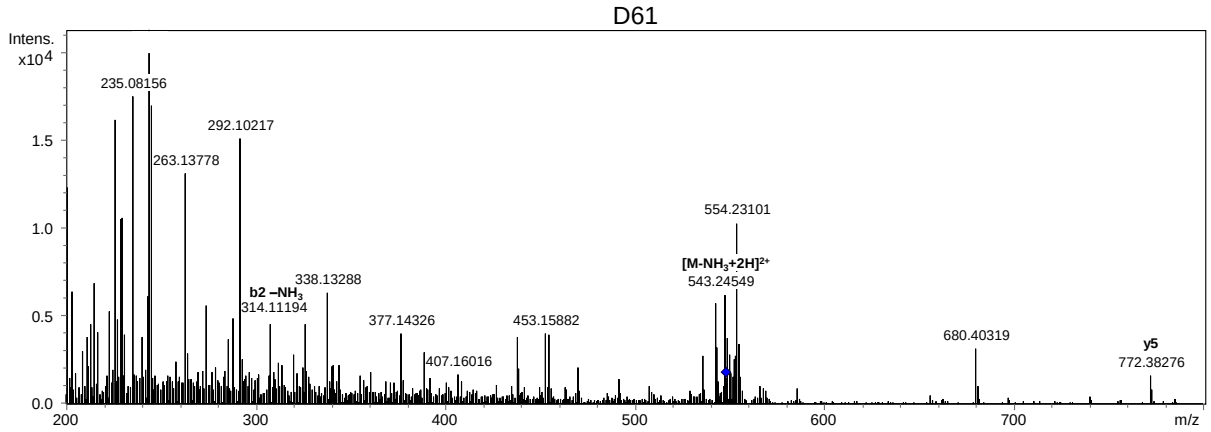

Figure S 24: MS^2 spectrum for D61.

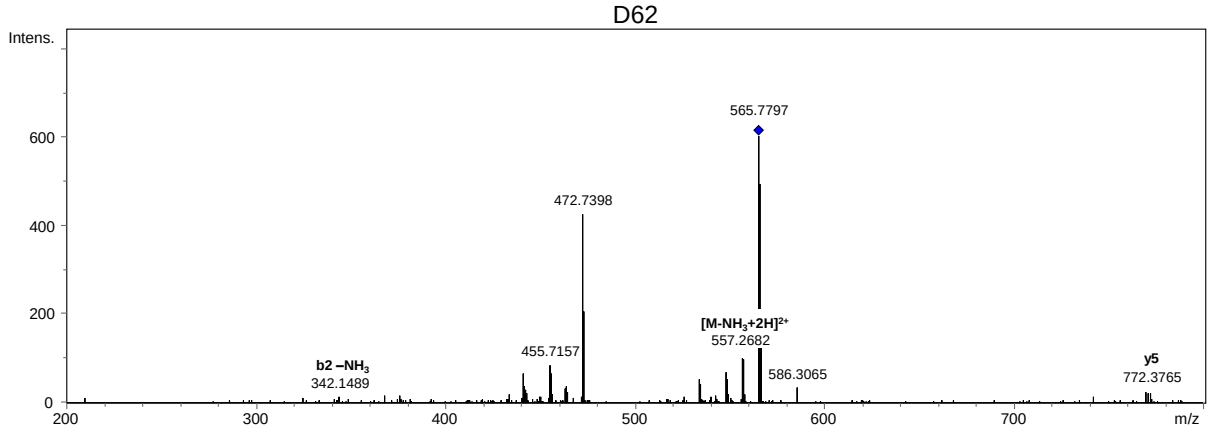

Figure S 25: MS^2 spectrum for D62.

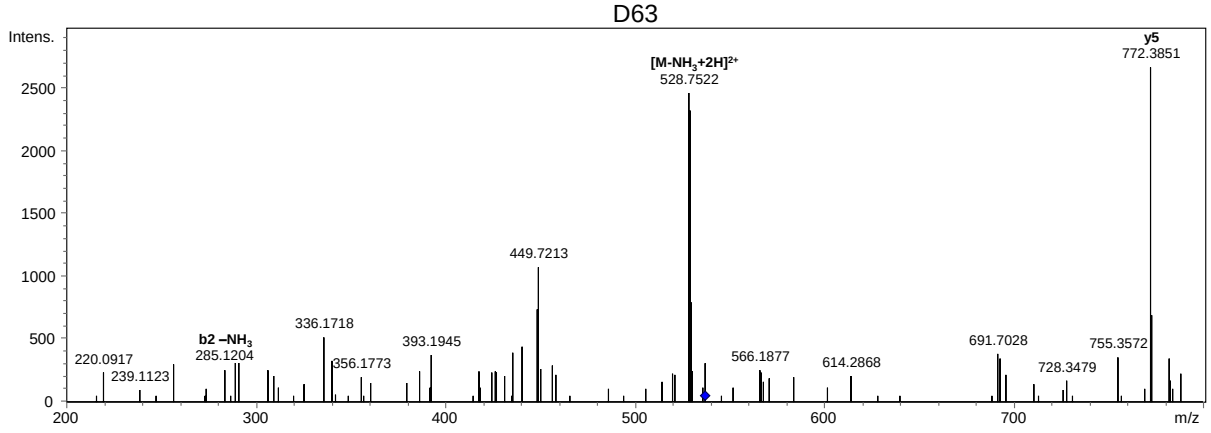

Figure S 26: MS^2 spectrum for D63.

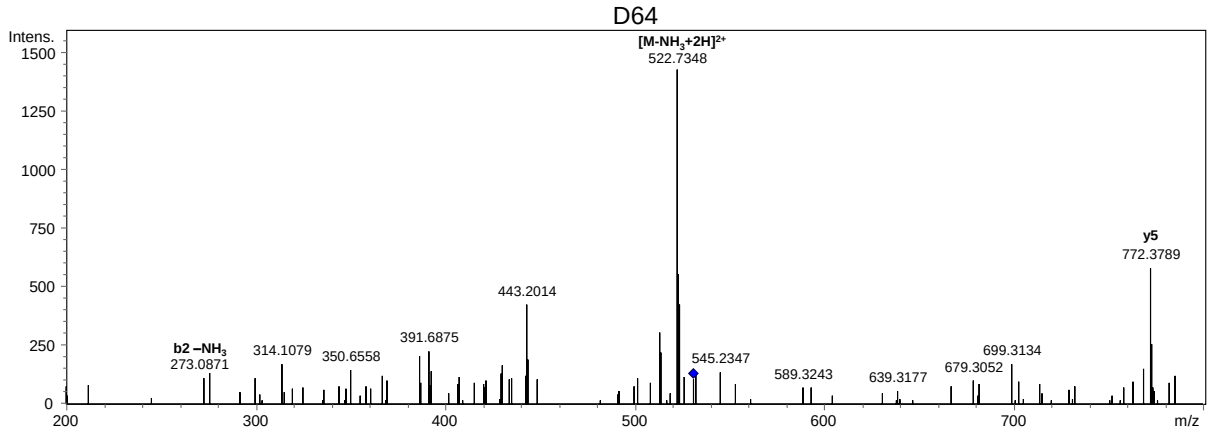

Figure S 27: MS^2 spectrum for D64.

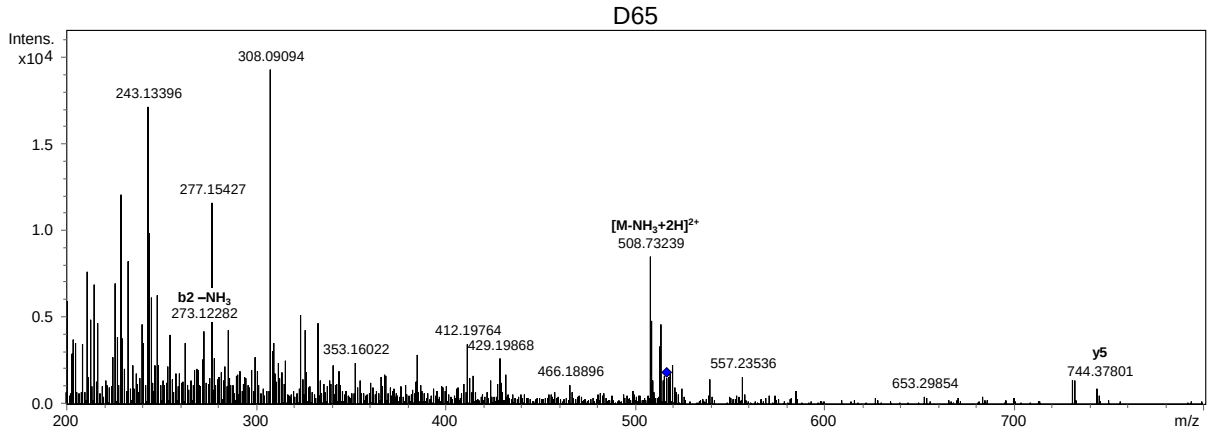

Figure S 28: MS^2 spectrum for D65.

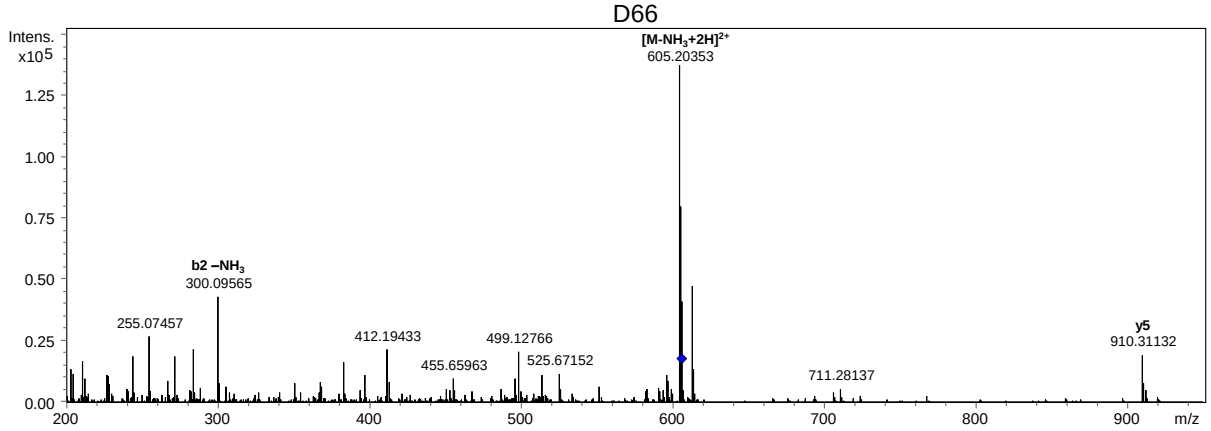

Figure S 29: MS^2 spectrum for D66.

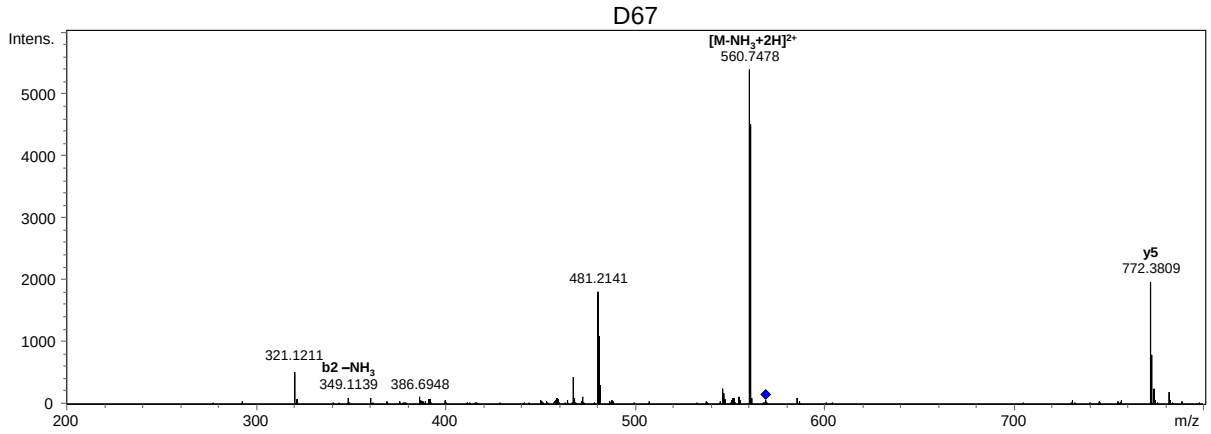

Figure S 30: MS^2 spectrum for D67.

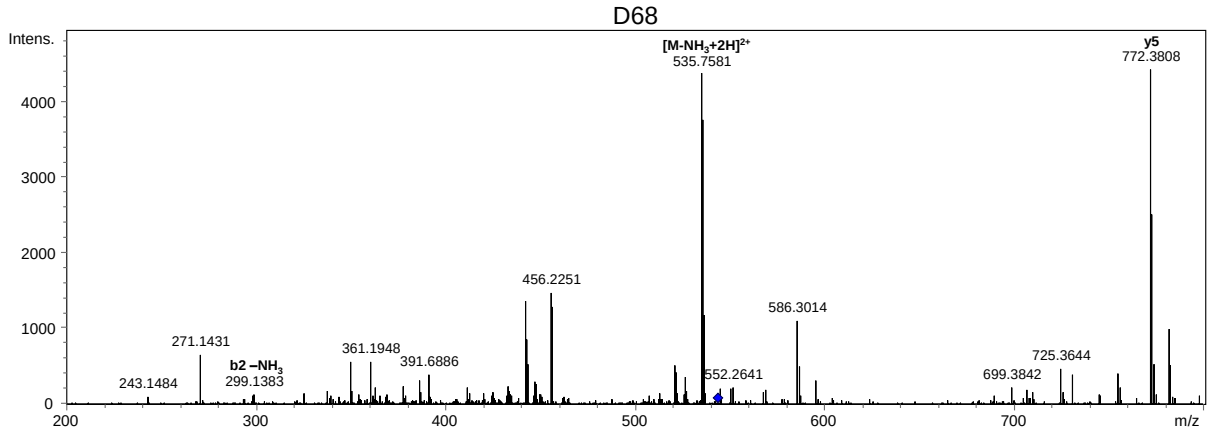

Figure S 31: MS^2 spectrum for D68.

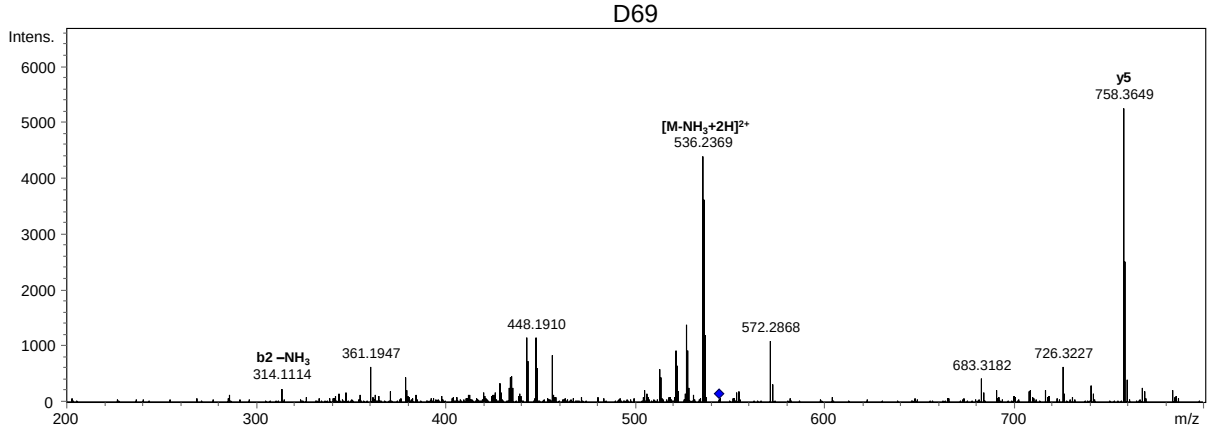

Figure S 32: MS^2 spectrum for D69.

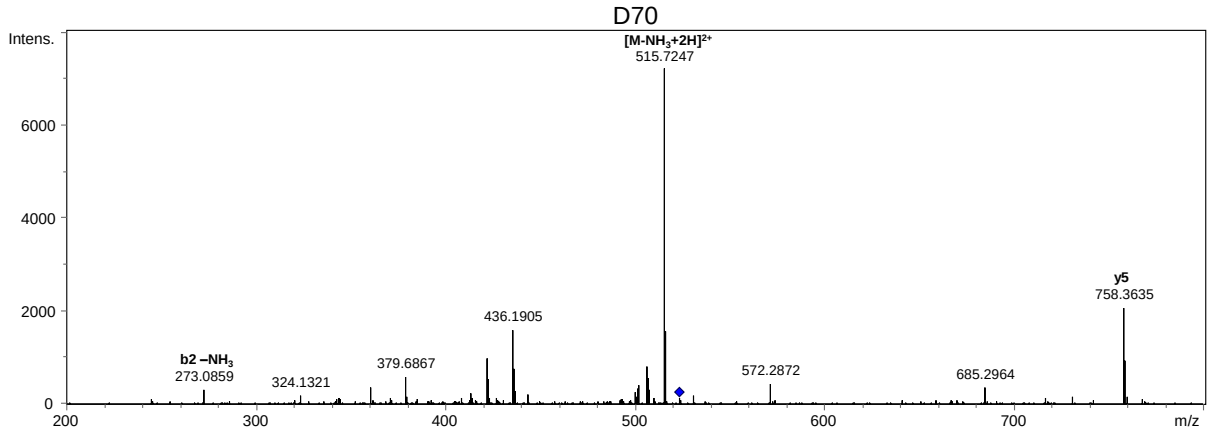

Figure S 33: MS^2 spectrum for D70.

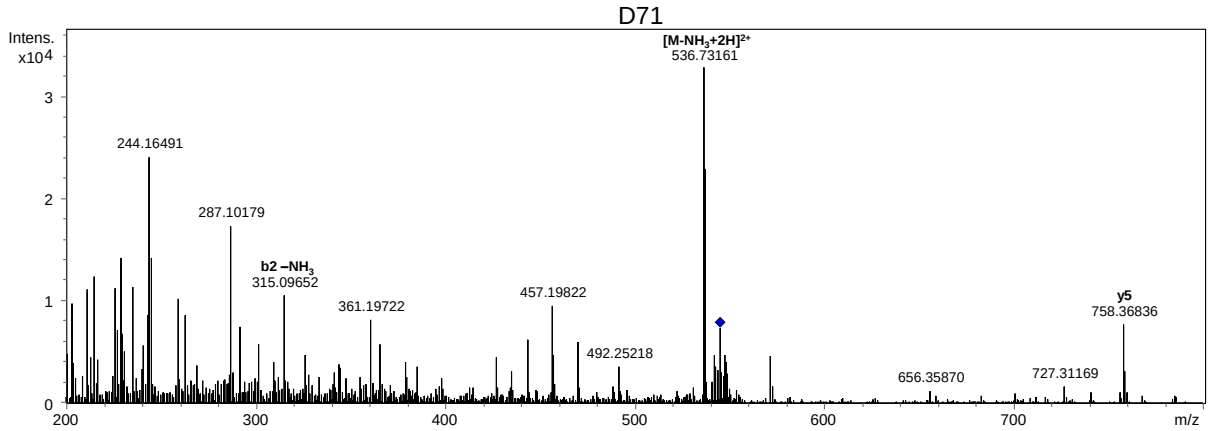

Figure S 34: MS^2 spectrum for D71.

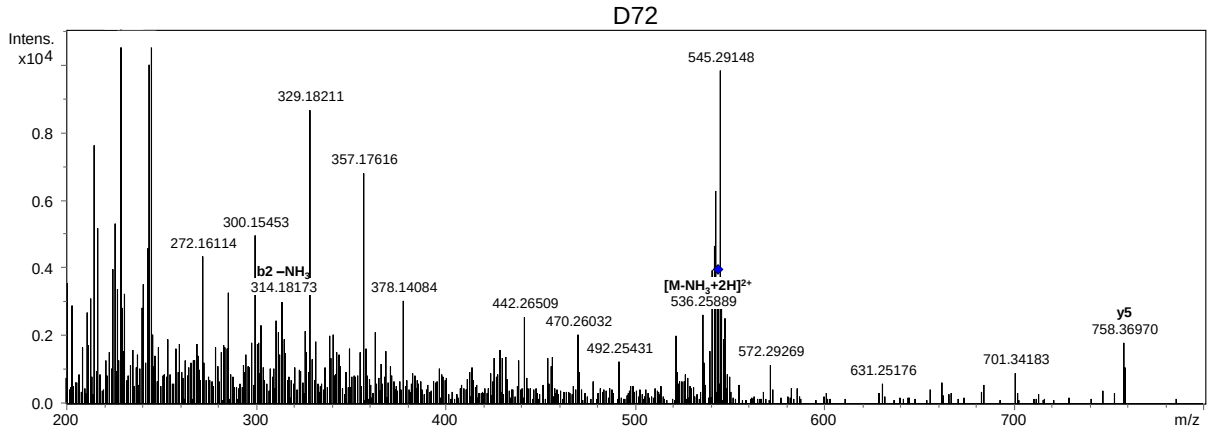

Figure S 35: MS^2 spectrum for D72.

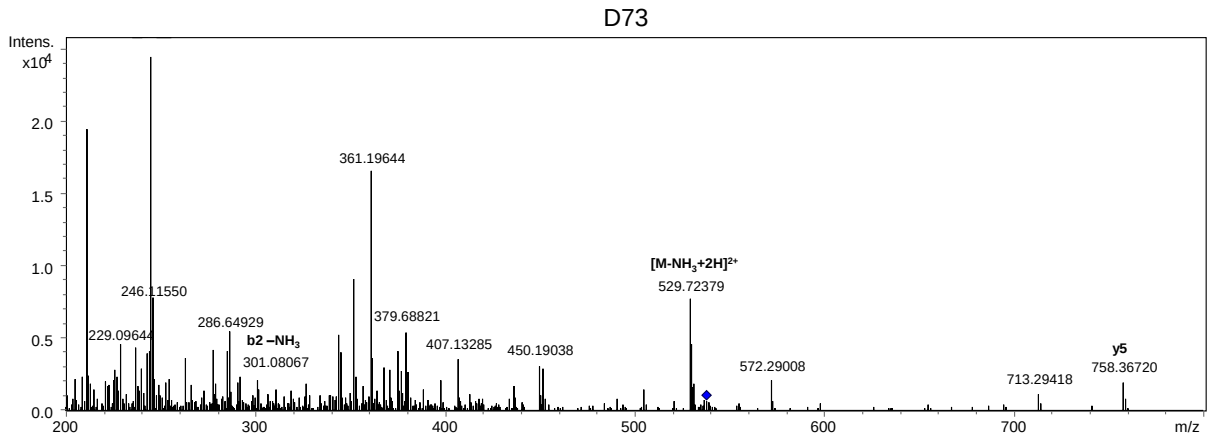

Figure S 36: MS^2 spectrum for D73.

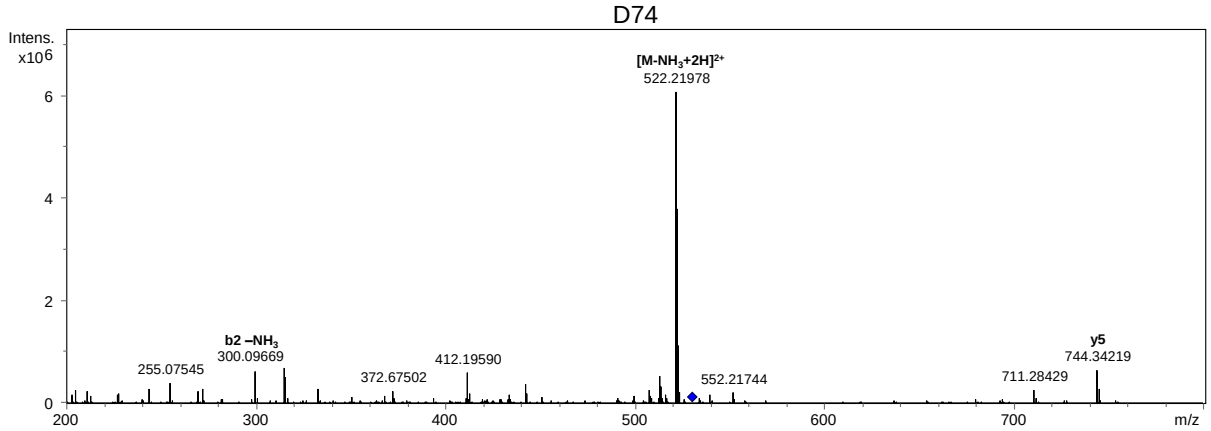

Figure S 37: MS^2 spectrum for D74.

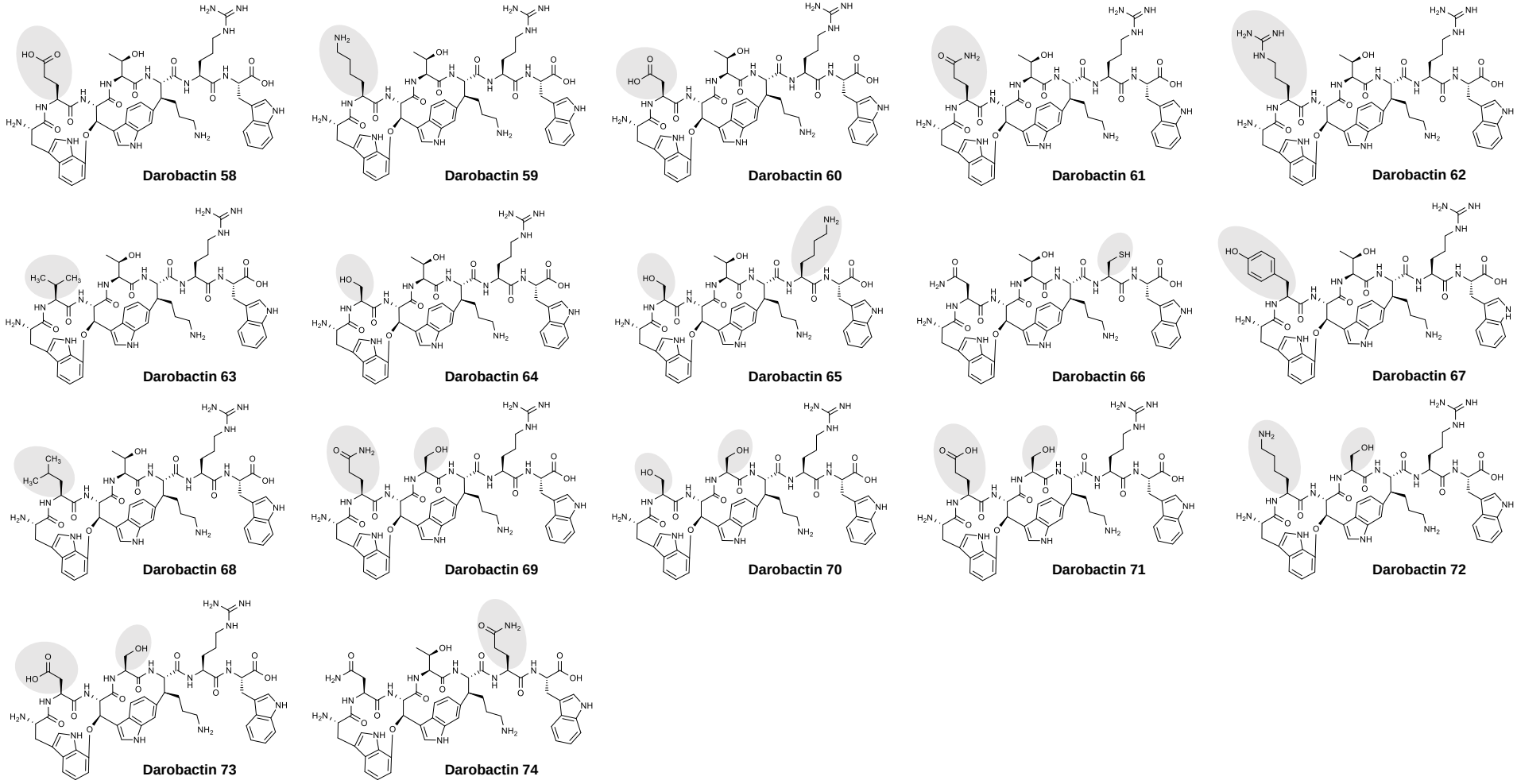

Figure S 38: Overview of all generated novel darobactin analogues. **D58** to **D74** are displayed and positions of heptapeptide with amino acid exchange compared to **D22** amino acid sequence were highlighted in grey. Structures were predicted using MS^2 analysis. **D69** was verified via NMR spectrometry (Table S 7, Figure S 39 – S44).

4. Antibiogram of clinical *P. aeruginosa* isolates

Table S 6: Antibiogram of clinical *P. aeruginosa* isolates. Antibacterial activity of **D22** and **D69** were evaluated in parallel with meropenem and ciprofloxacin (CIP) as controls (Table 4). The minimal inhibitory concentration (MIC) of **D22** and **D69** is comparable to the antibiotics Mereopenem and CIP. Broncheoalveolar lavage (BAL); permanent catheter urine (PK-urine); resistant (R); multi-resistant pathogen (MRP); multi-resistant Gram-negative pathogens with resistance against four of four groups of antibiotics (4MNGR).

		resistance profile, MIC [µg mL^{-1}]		
	material	MRP	Meropenem	CIP
P. aeroginosa 83979	BAL	4MRGN	> 16 (R)	> 4 (R)
P. aeroginosa 84389	PK-urine	4MRGN	16 (R)	4 (R)

5. Quantification of production

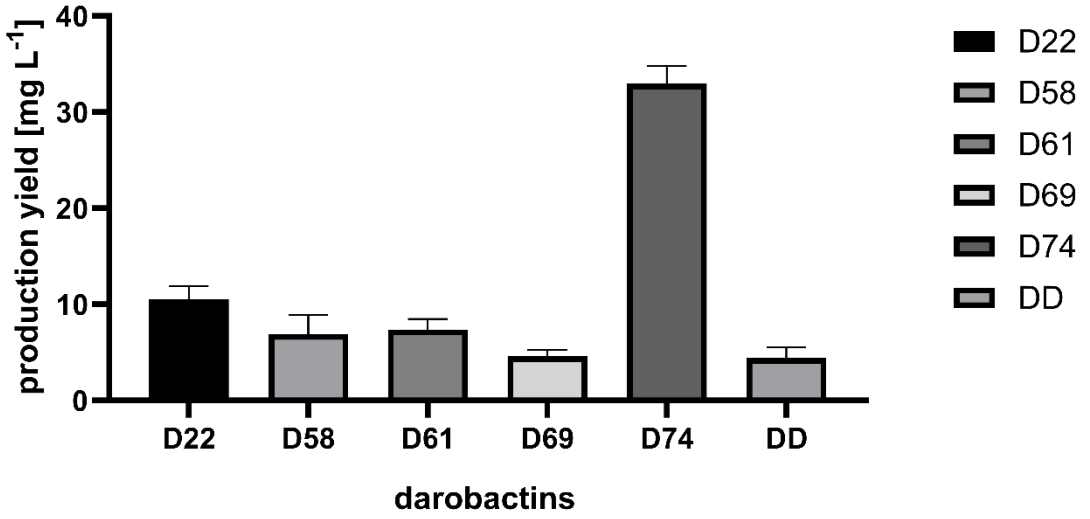

Figure S 39: Production yield of darobactin D22, D69 and D74. HPLC UV quantification of production yield was calculated by integration across the chromatographic UV peak area of each derivative. Eight (**D22**, **D69**), ten (**D74**) and twelve (**D58**, **D61**, **DD**) replicates were compared. The production yields of **D22** achieved 10.5 ± 0.9 mg per liter, of **D58** 6.9 ± 2.0 mg per liter, of **D61** 7.4 ± 1.1 mg per liter, of **D69** 4.6 ± 0.6 mg per liter**,** of **D74** 33 ± 1.7 mg per liter and of **DD** 4.4 ± 1.1 mg per liter, respectively.

6. NMR spectroscopic data

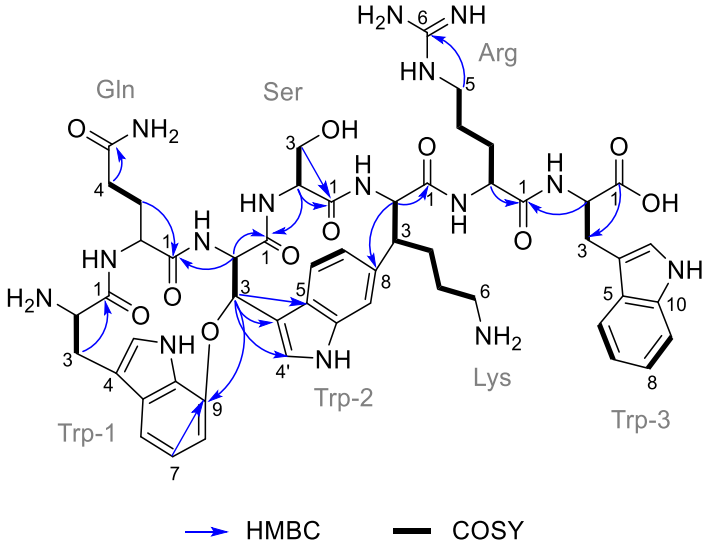

Table S 7: NMR Spectroscopic Data for D69[a].

	Pos.	δ_C[b], type	δ_H[c], (*J* in Hz)	COSY[d]	HMBC[e]
Trp-3	1	174.9, C	-	-	-
	2	53.7, CH	4.99, t (5.5)	3	1, 3, 4, Arg-1
	3	26.6, CH_2	3.63, m	2	1, 2, 4, 4', 5
	4'	124.0, CH	7.56, s	-	3, 4, 5, 9, 10
	4	109.0, C	-	-	-
	5	127.0, C	-	-	-
	6	118.1, CH	7.95, br d (7.5)	7	4, 5, 8, 10
	7	118.9, CH	7.45, m	6, 8	5, 6, 8, 9
	8	121.4, CH	7.53, m	7, 9	6, 10
	9	111.4, CH	7.81, br d (7.9)	8	5, 7
	10	135.9, C	-	-	-
Arg	1	171.9, C	-	-	-
	2	52.9, CH	4.60, br t (6.3)	3ab	1, 3
	3a	27.8, CH_2	1.88, m	2, 3b, 4	1, 2, 4, 5
	3b		2.02, m	2, 3a, 4	1, 2, 4, 5
	4	23.9, CH_2	1.74, m	3, 5	2, 5
	5	40.0, CH_2	3.34, m	4	3, 4, 6
	6	156.3, C	-	-	-
Lys	1	170.8, C	-	-	-
	2	59.7, CH	4.39, br d (10.3)	3	1, 3, 4, Ser-1, Trp2-8
	3	47.7, CH	3.21, m	2, 4b	2, 4
	4a	25.2, CH_2	1.82, m	4b, 6	6
	4b		2.12, m	4a, 3	-
	5	25.1, CH_2	2.04, m	4ab, 6	-
	6	38.9, CH_2	3.08, m	4a, 5	4
Ser	1	167.5, C	-	-	-
	2	53.7, CH	4.24, m	3ab	1, Trp2-1
	3a	61.6, CH_2	3.40, m	2	1
	3b		3.46, m	2	1
Trp-2	1	167.6, C	-	-	-
	2	62.9, CH	4.92, d (8.9)	3	1, 3, 4, Gln-1
	3	76.2, CH	6.39, br d (8.9)	2	2, 4, 4', 5, 9
	4'	123.8, CH	8.09, s	-	3, 4, 5, 10
	4	111.6, C	-	-	-
	5	124.6, C	-	-	-
	6	116.7, CH	7.69, d (7.3)	7	8, 10
	7	124.7, CH	7.18, d (7.3)	6	5, 9, Lys-3
	8	132.3, C	-	-	-
	9	110.1, CH	7.67, s	-	5, 8, 10, Lys-3
	10	136.6, C	-	-	-
Gln	1	169.0, C	-	-	-
	2	52.3, CH	3.33, m	3	1

	3	28.7, CH_2	1.78, m	4	-
	4	30.1, CH_2	2.20, m	3	2, 3, 5
	5	177.0, C	-	-	-
Trp-1	1	167.7, C	-	-	-
	2	54.3, CH	4.27, m	3ab	1, 3
	3a	25.9, CH_2	3.80, dd (13.3, 6.8)	2, 3b	1, 2, 4, 4', 5
	3b		3.54, m	2, 3a	2, 4, 4', 5
	4'	124.0, CH	7.59, s	-	4, 5, 9, 10
	4	107.8, C	-	-	-
	5	128.7, C	-	-	-
	6	119.6, CH	7.40, m	7	9, 10
	7	113.0, CH	7.44, m	6	5, 8, 9
	8	108.0, CH	7.44, m	-	7, 9, 10
	9	145.0, C	-	-	-
	10	128.6, C	-	-	-

[a]Recorded in D_2O/acetonitrile-d_3 (2:1) + 1% formic acid-d_4 at 318 K. [b]Acquired at 175 MHz, adjusted to the solvent signal of acetonitrile-d_3 (δ_C 118.69 ppm). [c]Acquired at 700 MHz, adjusted to the solvent signal of D_2O (δ_H 4.75 ppm). [d]Proton showing COSY correlation to indicated protons. [e]Proton showing HMBC correlation to indicated carbon.

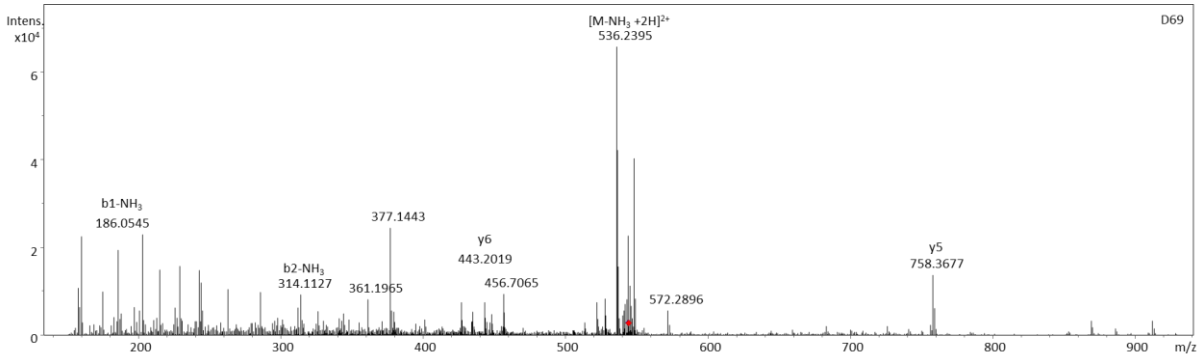

Figure S 40: MS^2 spectrum of D69. A red rhombus highlights the precursor ion with *m/z* 544.75490, which was picked for fragmentation. Furthermore, the $[M\text{-}NH_3+2H]^{2+}$ fragment and the characteristic b2-NH_3 and y5 fragment can be observed.

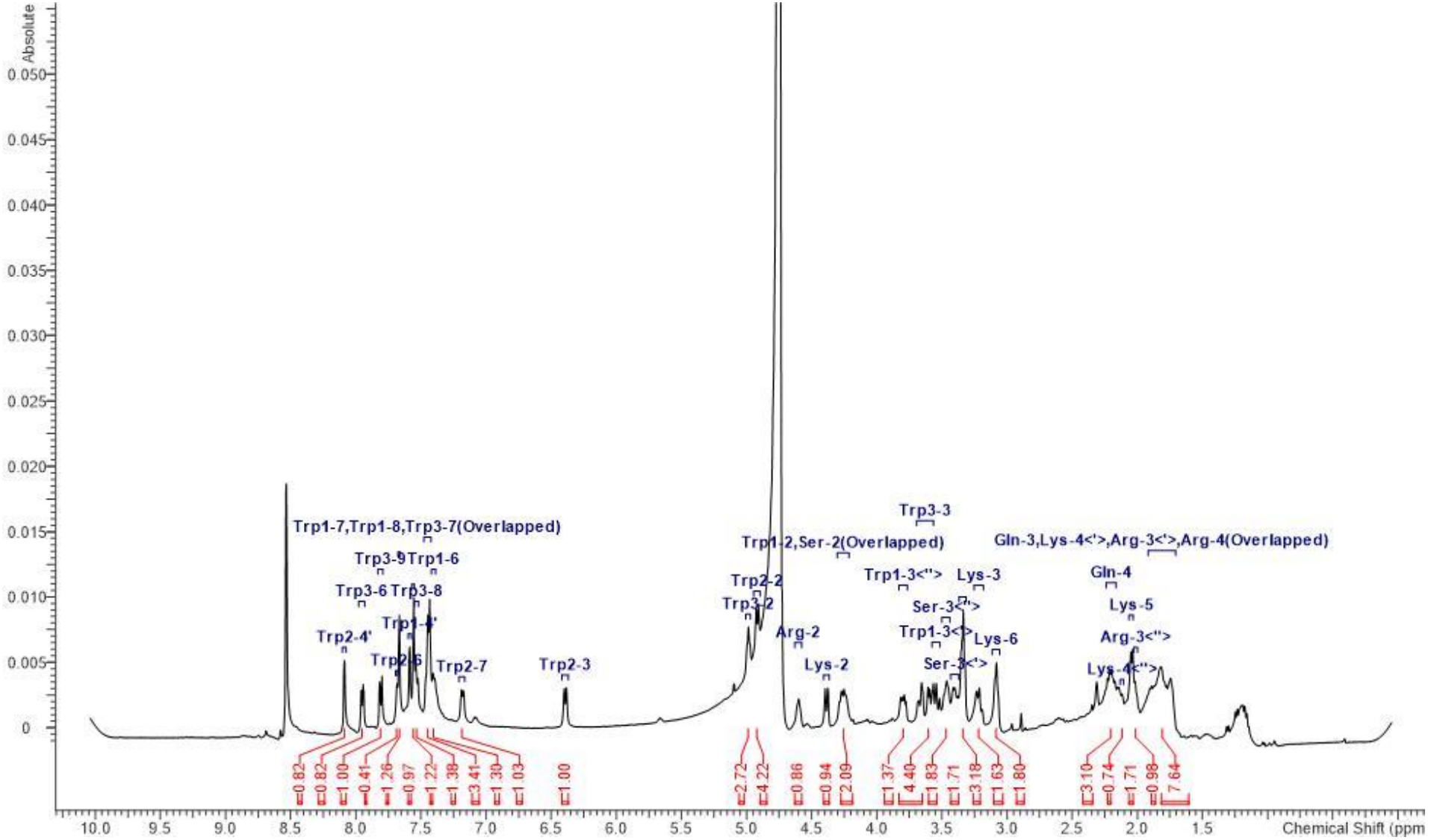

Figure S 41: ^{1}H NMR of D69 recorded in D_2O/acetonitrile-d_3 (2:1) + 1% formic acid-d_4 at 318 K.

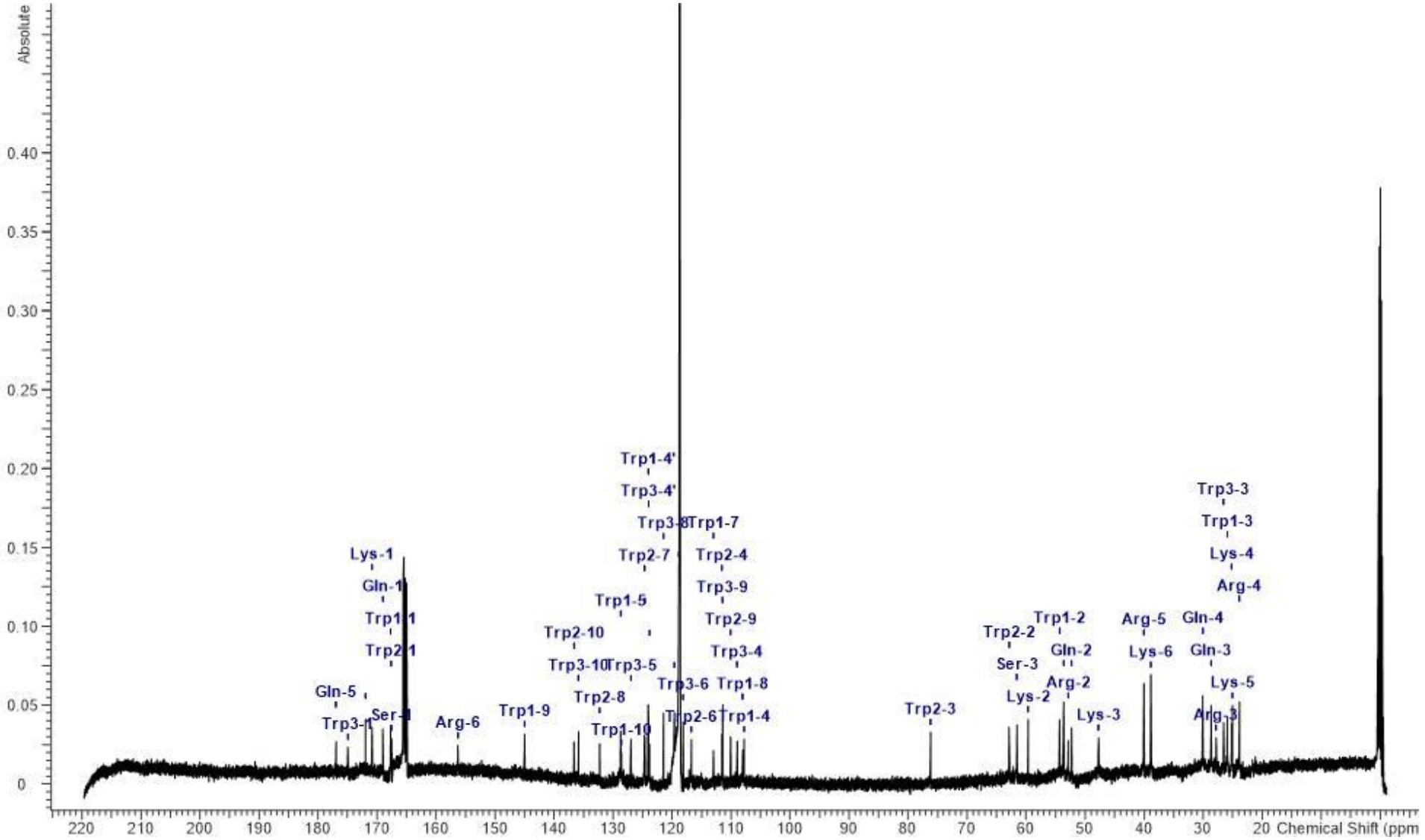

Figure S 42: ^{13}C NMR of D69 recorded in D_2O/acetonitrile-d_3 (2:1) + 1% formic acid-d_4 at 318 K.

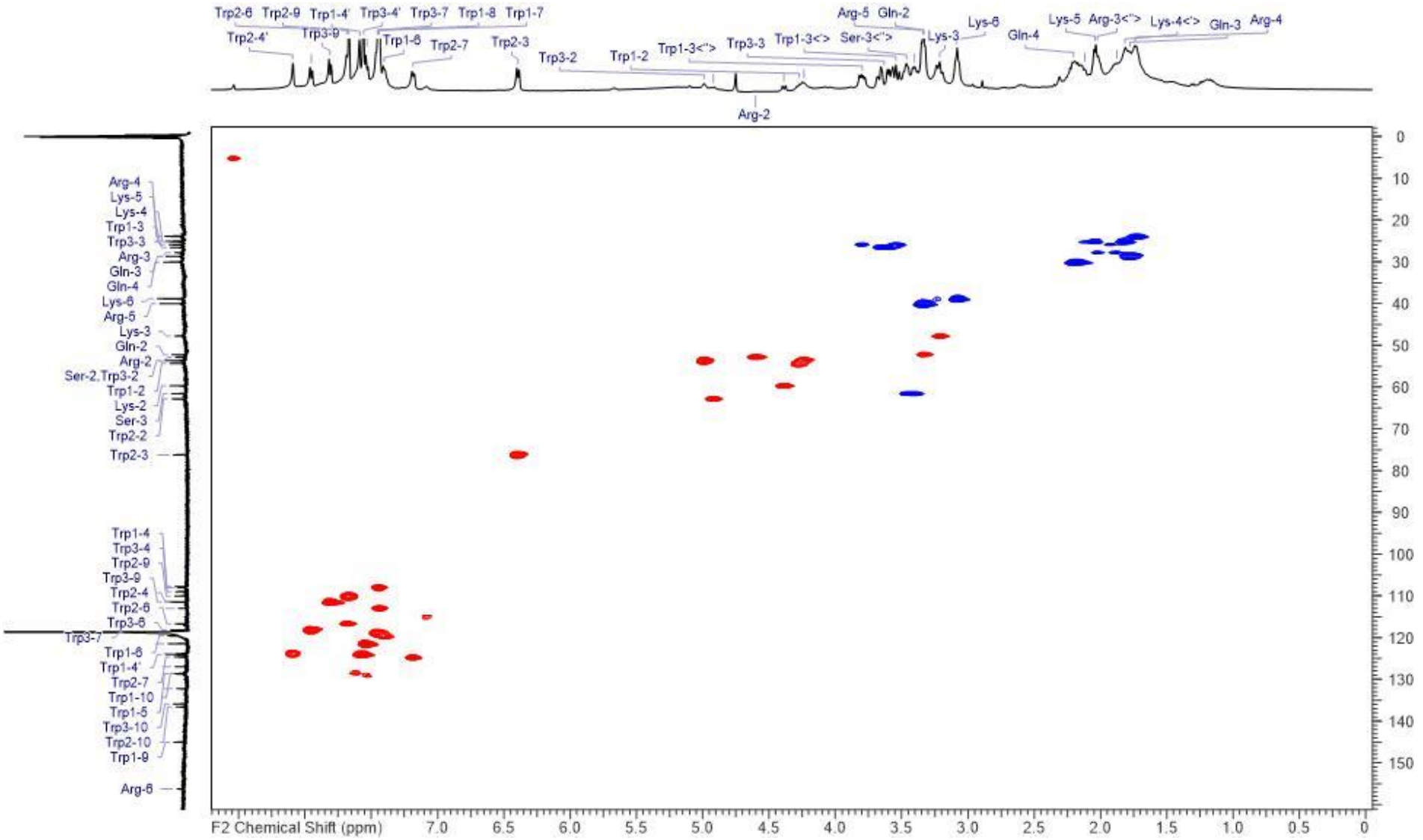

Figure S 43: HSQC NMR of D69 recorded in D_2O/acetonitrile-d_3 (2:1) + 1% formic acid-d_4 at 318 K.

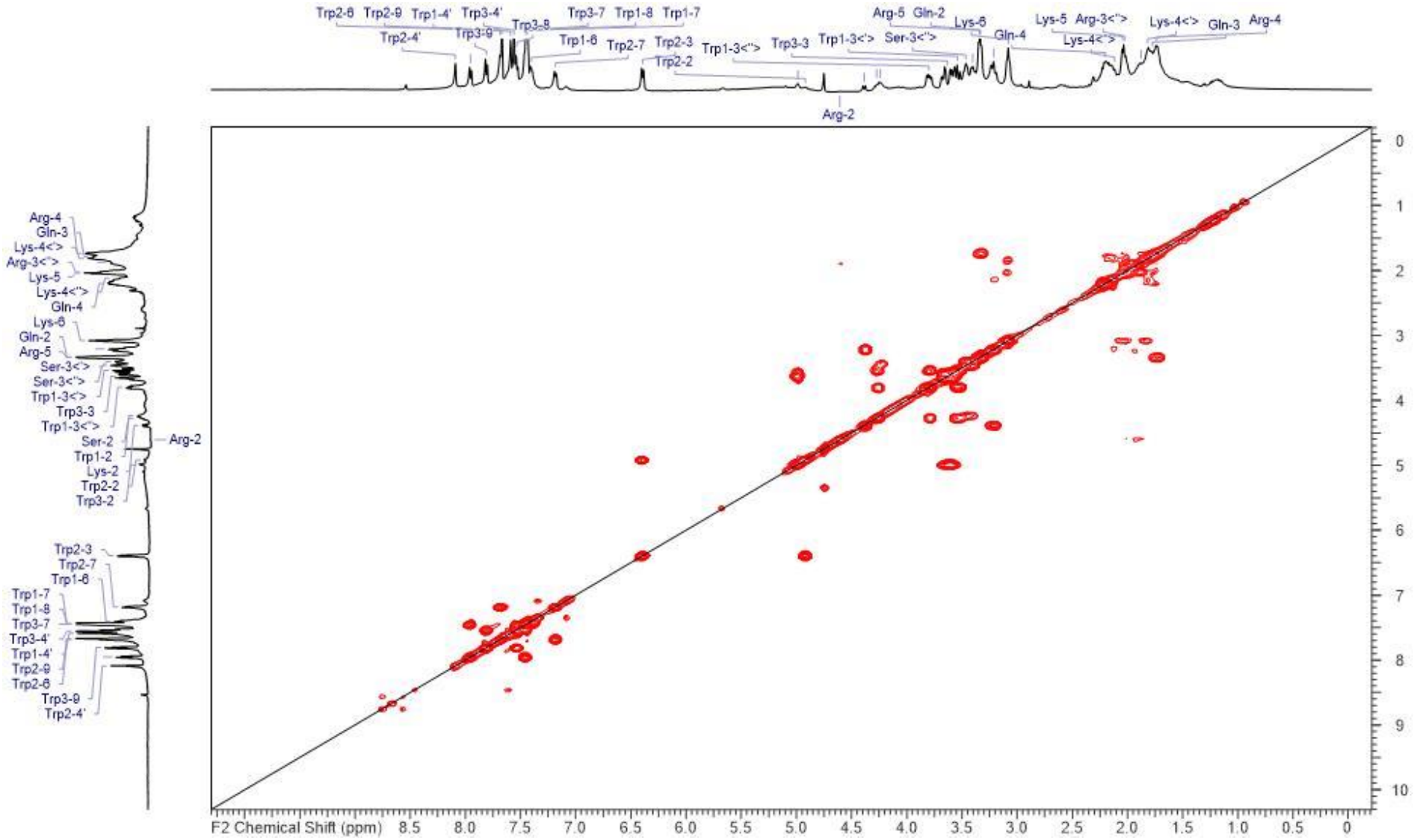

Figure S 44: COSY NMR of D69 recorded in D_2O/acetonitrile-d_3 (2:1) + 1% formic acid-d_4 at 318 K.

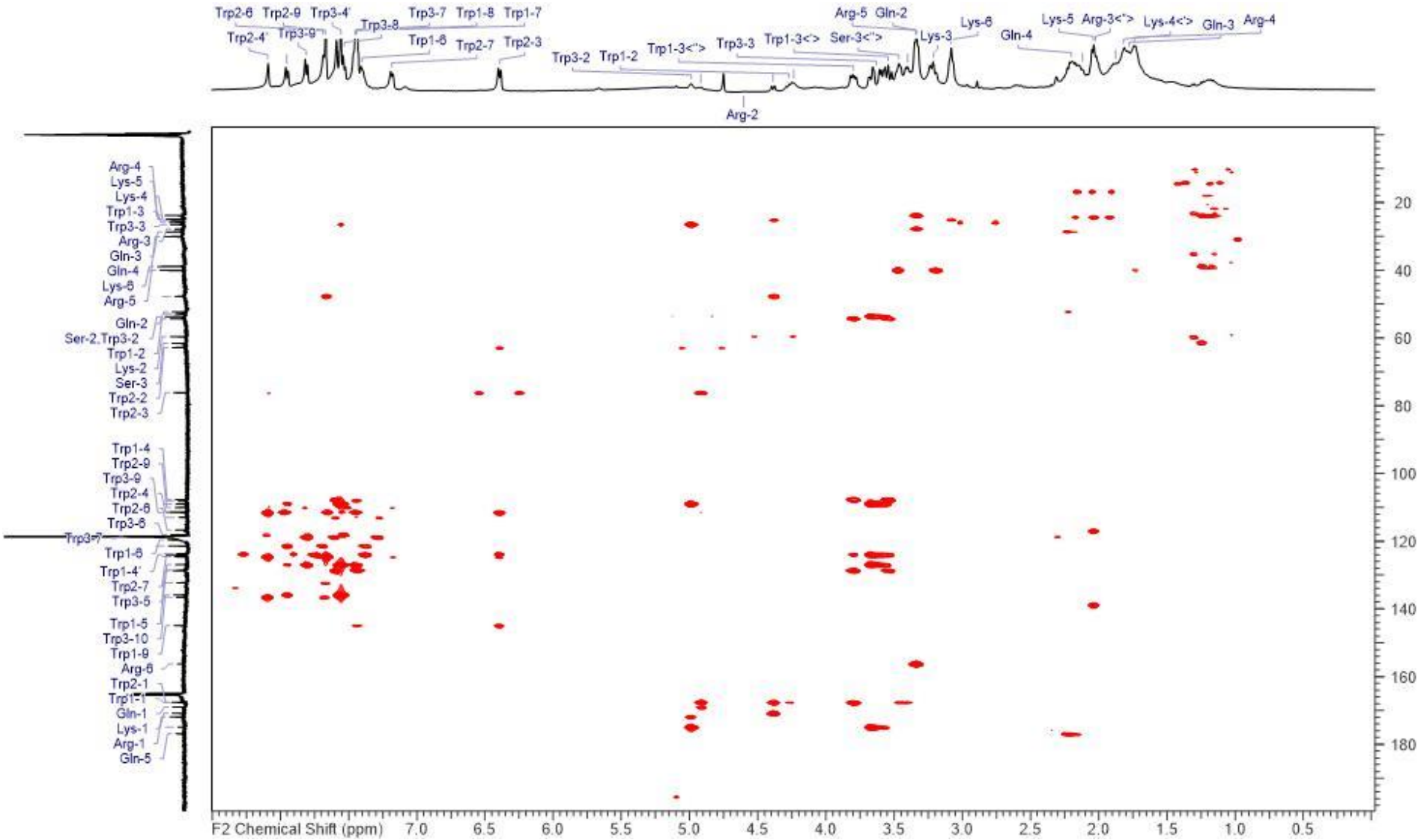

Figure S 45: HMBC NMR of D69 recorded in D_2O/acetonitrile-d_3 (2:1) + 1% formic acid-d_4 at 318 K.

7. HPLC traces of pure compounds

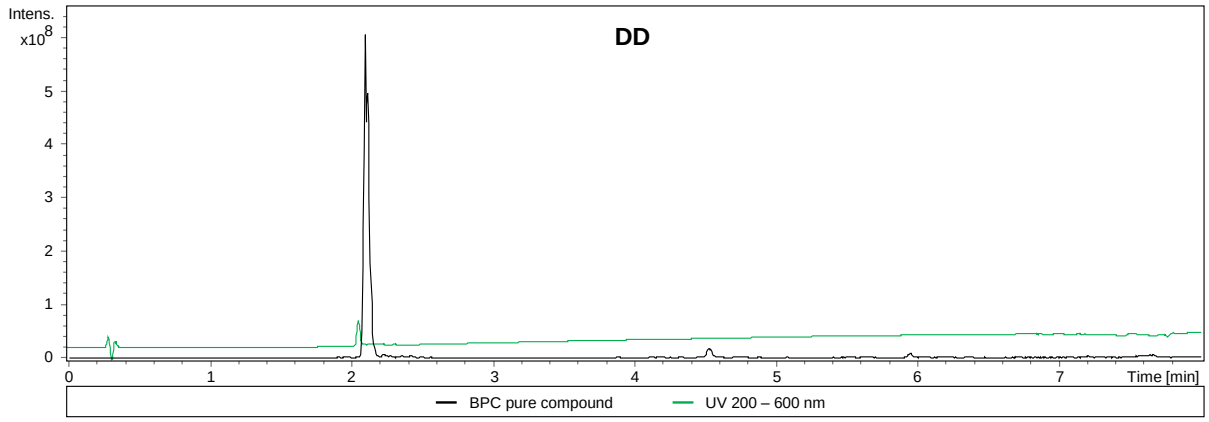

Figure S 46: Chromatogram of purified DD. The green trace shows the UV at 200–600 nm and the black trace shows the BPC. Acquired using amaZon speed.

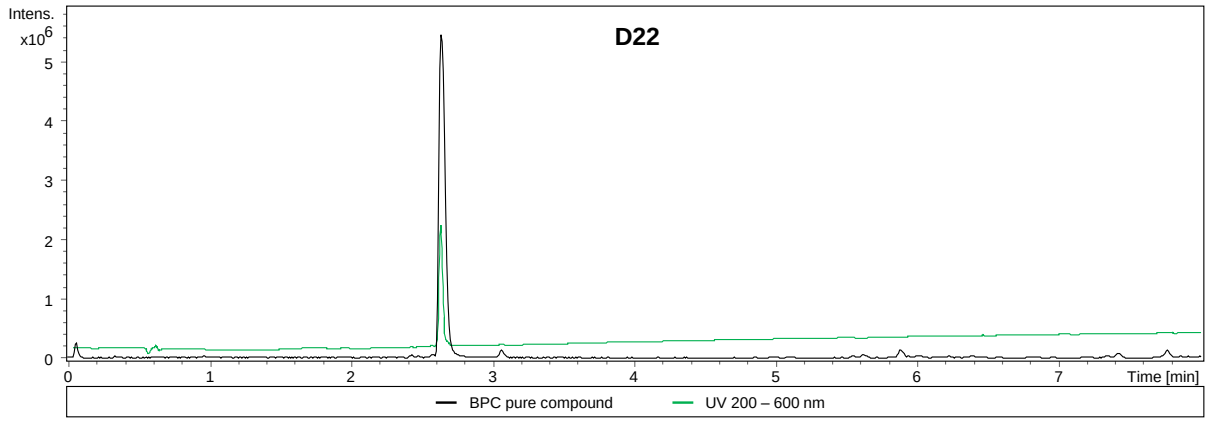

Figure S 47: Chromatogram of purified D22. The green trace shows the UV at 200–600 nm and the black trace shows the BPC. Acquired using maXis 4G.

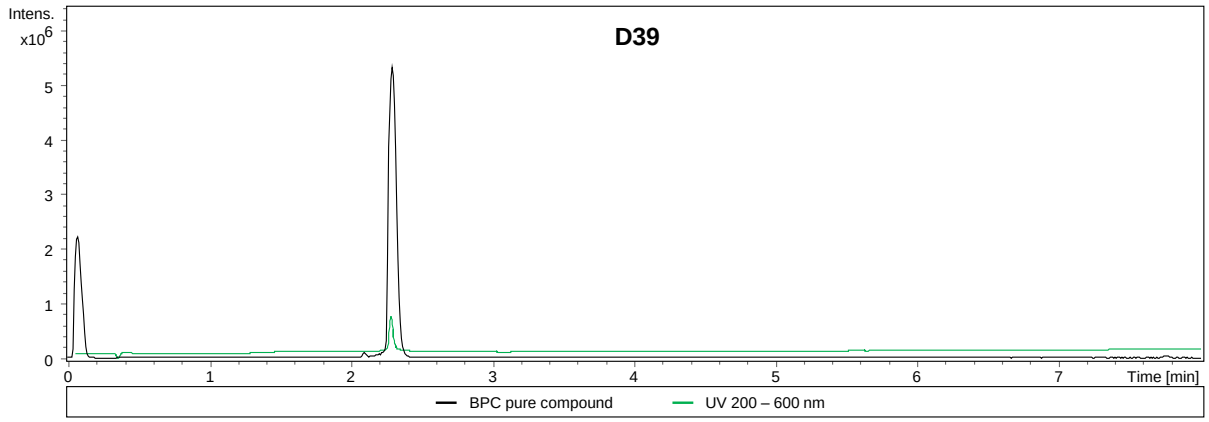

Figure S 48: Chromatogram of purified D39. The green trace shows the UV at 200–600 nm and the black trace shows the BPC. Acquired using maXis 4G.

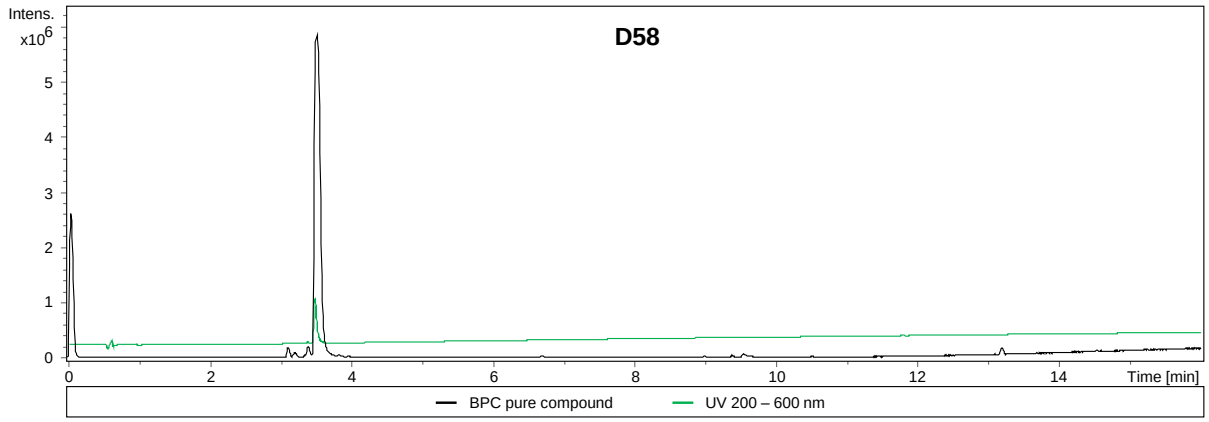

Figure S 49: Chromatogram of purified D58. The green trace shows the UV at 200–600 nm and the black trace shows the BPC. Acquired using maXis 4G.

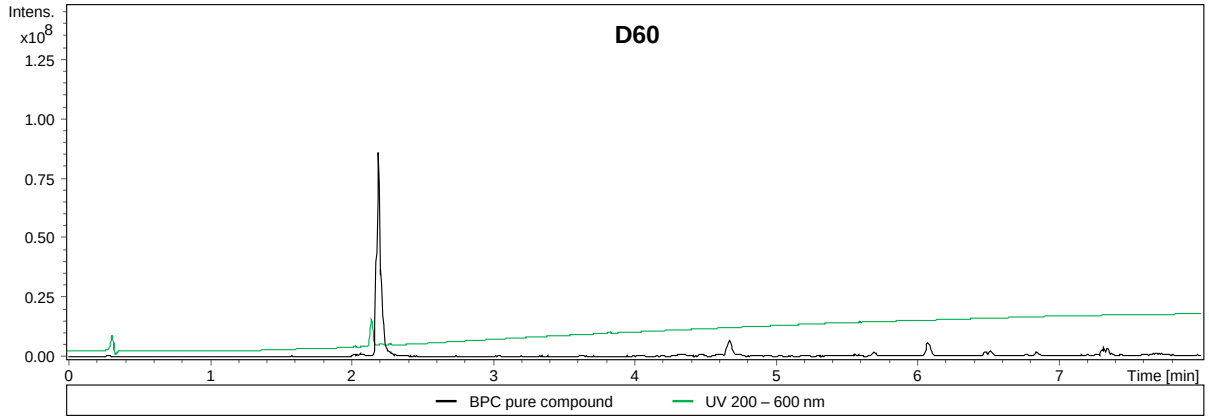

Figure S 50: Chromatogram of purified D60. The green trace shows the UV at 200–600 nm and the black trace shows the BPC. Acquired using amaZon speed.

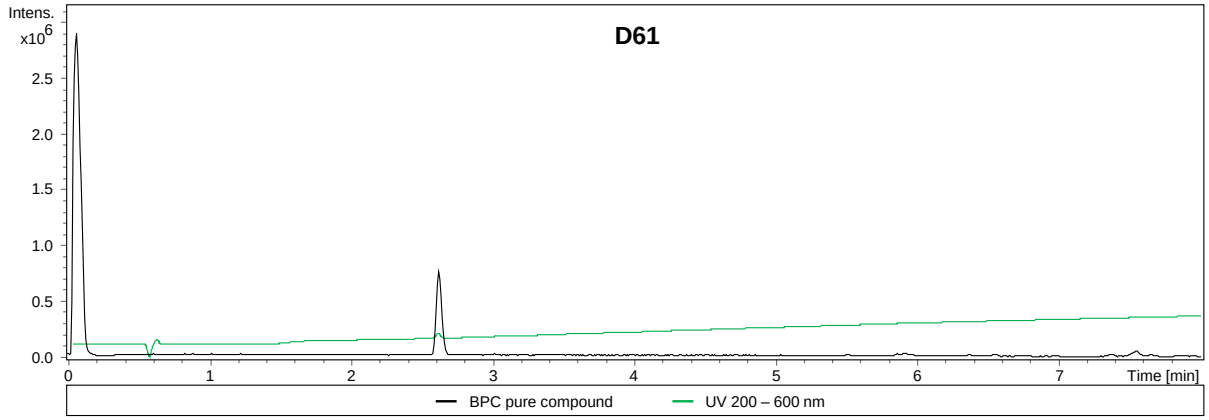

Figure S 51: Chromatogram of purified D61. The green trace shows the UV at 200–600 nm and the black trace shows the BPC. Acquired using maXis 4G.

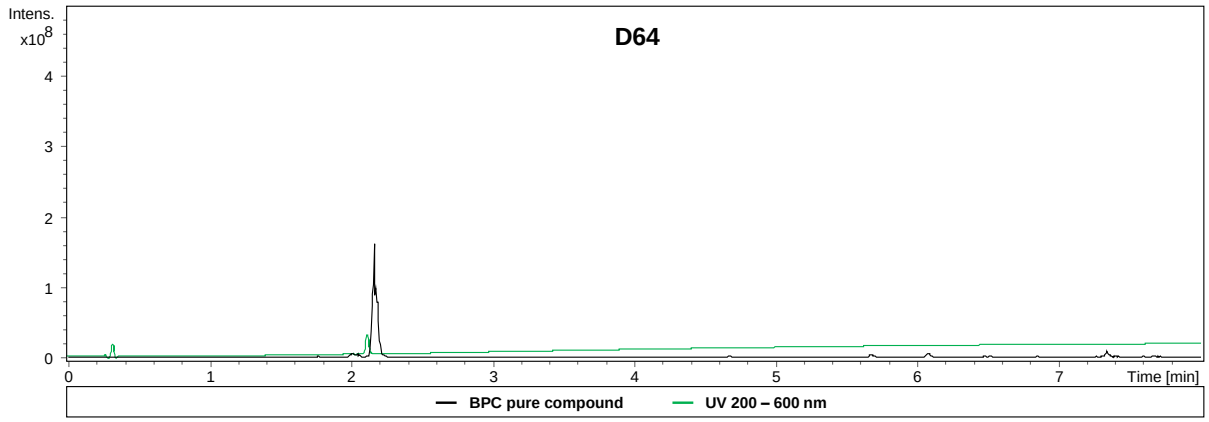

Figure S 52: Chromatogram of purified D64. The green trace shows the UV at 200–600 nm and the black trace shows the BPC. Acquired using amaZon speed.

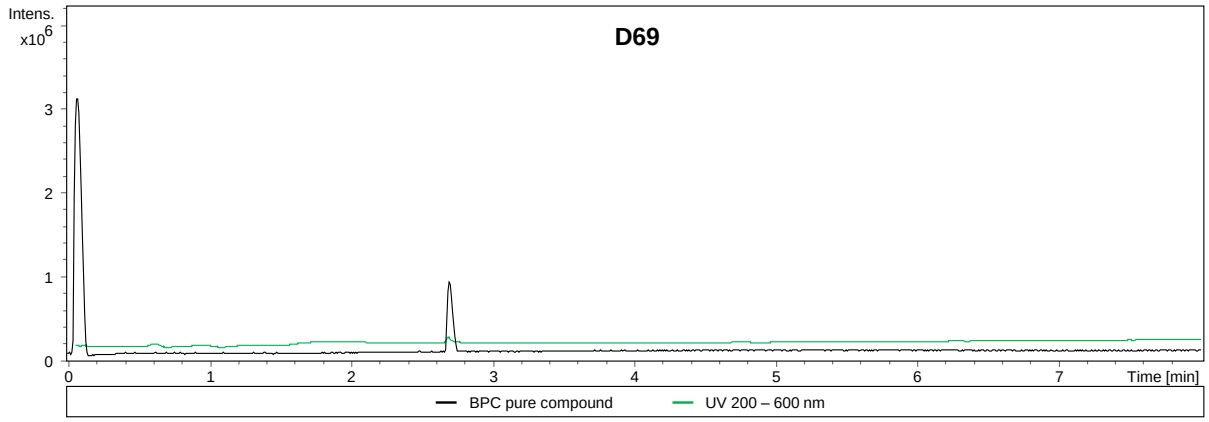

Figure S 53: Chromatogram of purified D69. The green trace shows the UV at 200–600 nm and the black trace shows the BPC. Acquired using maXis 4G.

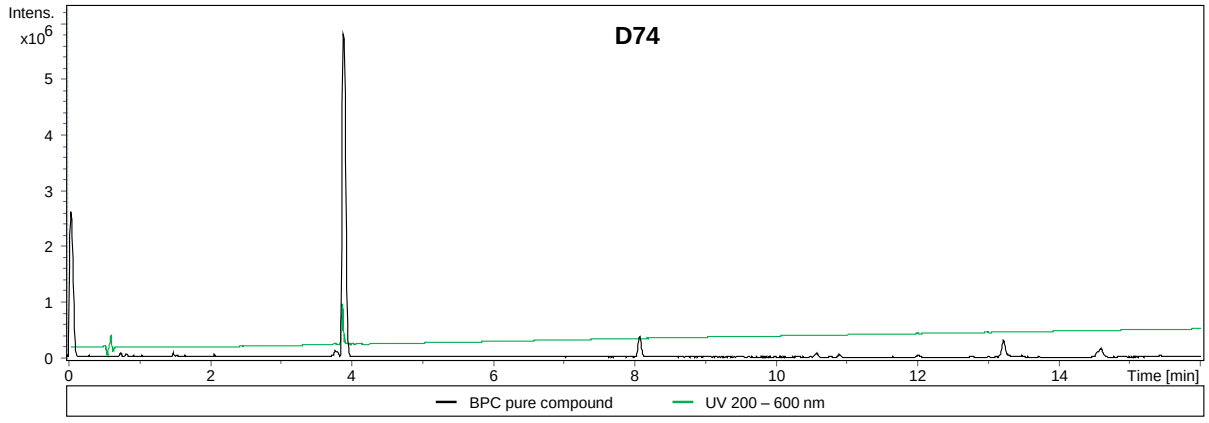

Figure S 54: Chromatogram of purified D74. The green trace shows the UV at 200–600 nm and the black trace shows the BPC. Acquired using maXis 4G.

References

(1) Goddard, T. D.; Huang, C. C.; Meng, E. C.; Pettersen, E. F.; Couch, G. S.; Morris, J. H.; Ferrin, T. E. UCSF ChimeraX: Meeting modern challenges in visualization and analysis. *Protein Science* **2018**, *27*, 14–25.

(2) Pettersen, E. F.; Goddard, T. D.; Huang, C. C.; Meng, E. C.; Couch, G. S.; Croll, T. I.; Morris, J. H.; Ferrin, T. E. UCSF ChimeraX: Structure visualization for researchers, educators, and developers. *Protein Sci.* **2021**, *30*, 70–82.

(3) Schrödinger. *The PyMOL Molecular Graphics System, Version 2.5.2*; Schrödinger, LLC, 2022.

(4) Pettersen, E. F.; Goddard, T. D.; Huang, C. C.; Couch, G. S.; Greenblatt, D. M.; Meng, E. C.; Ferrin, T. E. UCSF Chimera--a visualization system for exploratory research and analysis. *J. Comput. Chem.* **2004**, *25*, 1605–1612.

(5) Seyfert, C. E.; Porten, C.; Yuan, B.; Deckarm, S.; Panter, F.; Bader, C.; Coetzee, J.; Deschner, F.; Tehrani, K.; Higgins, P. G.*; et al.* Darobactins Exhibiting Superior Antibiotic Activity by Cryo-EM Structure Guided Biosynthetic Engineering. *Angew. Chem. Int. Ed.* **2022**, *62*, e202214094.

(6) Groß, S.; Panter, F.; Pogorevc, D.; Seyfert, C. E.; Deckarm, S.; Bader, C. D.; Herrmann, J.; Müller, R. Improved broad-spectrum antibiotics against Gram-negative pathogens via darobactin biosynthetic pathway engineering. *Chem. Sci.* **2021**, *12*, 11882–11893.